Balancing growth amidst salinity stress – lifestyle perspectives from the extremophyte model *Schrenkiella parvula*

Kieu-Nga Tran[1↟], Pramod Pantha[1↟], Guannan Wang[1↟], Narender Kumar[1,2↟], Chathura Wijesinghege[1], Hyewon Hong[3], John C. Johnson[1], Ross Kelt[1], Megan G. Matherne[1], Ashley Clement[1], David Tran[4], Colt Crain[5], Dong-Ha Oh[1], Prava Adhikari[1], Maryam Foroozani[1,6], Patrick Finnegan[7], David Longstreth[1], John C. Larkin[1], Aaron P. Smith[1], Maheshi Dassanayake[1,*]

[1]Department of Biological Sciences, Louisiana State University, Baton Rouge, LA 70803, USA
[2]Current address: Department of Botany and Plant Pathology and Center for Plant Biology, Purdue University, West Lafayette, IN 47907, USA
[3]Department of Plant Biology, University of Illinois, Urbana-Champaign, IL 61801, USA
[4]Department of Biochemistry & Department of Psychology, University of Miami, Coral Gables, FL 33146, USA
[5]Louisiana School for Math, Science and the Arts, Natchitoches, LA 71457, USA
[6]Current address: Department of Biology, Emory University, GA 30322, USA
[7]School of Biological Sciences, University of Western Australia, Perth, 6009, Australia

[↟]Equal contribution
*Address correspondence to: maheshid@lsu.edu

Keywords: Extremophyte, abiotic stress adaptations, tradeoffs in growth and stress tolerance, genomics, *Schrenkiella parvula*, salt stress

Abstract

The use of extremophyte models to select growth promoting traits during environmental stresses is a recognized yet an underutilized strategy to design stress-resilient plants. *Schrenkiella parvula*, a leading extremophyte model in Brassicaceae, can grow and complete its life cycle under multiple environmental stresses, including high salinity. While *S. parvula* is

equipped with foundational genomic resources to identify genetic clues that potentially lead to stress adaptations at the phenome level, a comprehensive physiological and structural characterization of salt stress responses throughout its lifecycle is absent. We aimed to identify the influential traits that lead to resilient growth and strategic decisions to ensure survival of the species in an extreme environment, and examined salt-induced changes in the physiology and anatomy of *S. parvula* throughout its life cycle across multiple tissues. We found that *S. parvula* maintains or even enhances growth during various developmental stages at salt stress levels known to inhibit growth in *Arabidopsis thaliana* and most crops. The resilient growth of *S. parvula* was associated with key traits synergistically allowing continued primary root growth, expansion of xylem vessel elements across the root-shoot continuum, and the high capacity to maintain tissue water levels by developing larger and thicker leaves while facilitating continued photosynthesis during salt stress. In turn, the stress-resilient growth during the vegetative phase of *S. parvula* allowed a successful transition to a reproductive phase via early flowering followed by the development of larger siliques with viable seeds on salt-treated plants. Additionally, the success of self-fertilization in early flowering stages was dependent on salt-induced filament elongation. Our results suggest that the maintenance of leaf water status and enhancement of selfing in early flowers to ensure reproductive success are among the most influential traits that contribute to the extremophilic lifestyle of *S. parvula* in its natural habitat.

Introduction

Balancing plant growth with environmental stress responses is a constant challenge all plants have adaptations, of which extremophytes have epitomized. Soil characteristics, water availability, and light and temperature regimes set boundaries for plant growth and dictate how plants complete their life cycles. Therefore, extremophytes, which are plants adapted to wider ranges in environmental conditions, provide insights on evolutionarily-tested lifestyle strategies proven successful in extreme or highly variable environments (Lloyd and Oreskes, 2018; Rodell *et al*., 2018; Schlenker and Auffhammer, 2018). Knowledge transfer from extremophyte-focused studies to design innovative crops optimized for growth amidst environmental stress is imperative when envisioning global food security and expansion of agricultural lands into

reclaimed or marginal lands in an era of climate change (Oh *et al*., 2012; Bechtold, 2018; Kazachkova *et al*., 2018; Zandalinas *et al*., 2021). The recent explosion of tools for genome exploration and engineering in a wider range of plants makes this an ideal time for mining representative extremophyte traits.

Schrenkiela parvula (Schrenk) D.A.German & Al-Shehbaz (also referred to in literature as *Thellungiella parvula* or *Eutrema parvulum*) (WCSP; IPNI, 2021) is a leading extremophyte model in the Brassicaceae family that shares many features with the premier model, *Arabidopsis thaliana*, (Zhu, 2015; Ali and Yun, 2017; Kazachkova *et al*., 2018; Krämer, 2018) (Fig 1). In the ten years following its genome release, *S. parvula* has been developed as a model system equipped with primary molecular tools to explore genetic mechanisms underlying plant abiotic stress tolerance (Dassanayake *et al*., 2011; Oh *et al*., 2014; Wang *et al*., 2018; Pantha *et al*., 2021; Wang *et al*., 2021). *S. parvula* shows a remarkable tolerance to high salinity compared to closely related Brassicaceae species (Orsini *et al*., 2010) and is categorized as a halophyte based on its capacity to complete life cycle in salinities at 200 mM or higher NaCl (Flowers and Colmer, 2008). In addition to high sodium, *S. parvula* is also uniquely adapted to multiple edaphic factors found in its native range which include high boron, potassium, and lithium, among other salts, reaching levels toxic for most crops (Helvaci *et al*., 2004; Oh *et al*., 2014; Hajiboland *et al*., 2018; Tug *et al*., 2019). Its preferential distribution near saline lakes in the Irano-Turanian region provides a robust extremophyte model to investigate multiple environmental stresses often found as compound stresses in many marginal agricultural landscapes or agricultural lands abandoned due to anthropogenic causes (Ozfidan-Konakci *et al*., 2015; Zandalinas *et al*., 2021).

New genome editing methods and advances in data science are expected to revolutionize future crop development in parallel to growing efforts to identify candidate genes that could enhance plant stress tolerance, and extremophytes have great potential as a key resource (Gómez *et al*., 2019; Basso and Antle, 2020; Solis *et al*., 2020; Barros *et al*., 2021; Gao, 2021). Nevertheless, critical physiological assessments are needed to identify plastic and induced stress responses that complement constitutive stress responses in extremophytes and the extent of trade-offs between plant growth and stress tolerance to assess how selected

traits, genes, or pathways affect short or long term plant growth and fitness. Such studies are lagging for all the leading extremophyte models compared to the breadth of tools and molecular resources available to identify candidate genes from these models.

For *S. parvula*, despite a growing body of genomic resources (Jarvis *et al*., 2014; Ali *et al*., 2018; Wang *et al*., 2021), a systematic study that illustrates its life history, physiological, and structural features associated with adaptations to survive environmental stresses, primarily represented by salt stress, is absent. In this study, we evaluated *S. parvula* stress adaptations at both structural and physiological levels during major developmental phases. We assessed adaptations influential in balancing growth with stress tolerance of this prime extremophyte model and identified induced adaptive traits that emerge as the most prominent features in a multivariate space across developmental stages, tissue types, and response types that we propose as hallmarks of a stress-adapted lifestyle.

Materials and Methods

Plate grown plants

S. parvula (Lake Tuz ecotype) and *A. thaliana* (Col-0 ecotype) seeds were surface sterilized with 50% bleach (sodium hypochlorite, 5.25%) (V/V) containing 2-3 drops of Tween-20 (MP Biomedicals, LLC, Aurora, Ohio, USA) for 5 minutes, 70% ethanol for 30 seconds, and immediately washed 4-5 times with sterilized distilled water. Sterilized seeds were stratified at 4°C for four to five days before germinating on 1/4 Murashige and Skoog (MS) (Murashige and Skoog, 1962) medium solidified with Phyto agar (0.8%) (Plant Medium) without sucrose on the medium unless it is mentioned in the figure caption. The plates were kept at 100-150 µmol $m^{-2}s^{-1}$ photosynthetic photon flux density under 12/12-h photoperiod at 23°C.

Primary, lateral root growth, and root hair quantification. 5-day-old seedlings grown in 1/4 MS medium were transferred to 1/4 MS supplemented with different concentrations of NaCl. We quantified primary root length, number of lateral roots, and lateral root density from seedlings grown on NaCl plates for 7, 10, and 13 days. We measured the average length of the 10 longest root hairs, and used it as a proxy for root hair growth. Plates were photographed

either with a camera (Nikon) or a microscope (Zeiss Neolumar S 1.5 X FWD 30 mm), and analyzed with ImageJ (Ferreira and Rasband, 2012).

Freezing, chilling, and heat stress on seedling survival. 5 day-old seedlings grown on 1/4 MS were subjected to heat stress at 38°C for 6, 18 and 24 h, chilling stress at 4°C for 24 h, or freezing stress at 0°C for 12 h. After the treatments, the seedlings were returned to normal growth condition for recovery for 5 days. Seedlings were considered to have survived if roots continued to grow without visible chlorosis of the cotyledons after the recovery period.

Root bending assay. Sterilized seeds were germinated on 1/2 MS media. Seeds were placed on a straight line, and the plates were rotated 45-degree angle from the plated seed line and 85-degree incline from the ground. After 5 days, we cut the lower part of 1/2 MS media at 1 cm below the root tips and filled in with 1/2 MS media supplemented with 200 mM NaCl. The plates were returned to the original orientation in the growth room and monitored for an additional 5 days.

Germination assay. Sterilized seeds were germinated on 1/4 MS media supplemented with different concentrations of NaCl, KCl, LiCl, or H_3BO_3. Germination rates were recorded three days after planting. Seeds were counted as germinated if the radicle emerged, no matter whether they further developed into seedlings. To check the viability of ungerminated seeds, *S. parvula* seeds that failed to germinate on high NaCl and KCl plates were transferred back to 1/4 MS media and monitored for an additional two weeks.

Hydroponically grown plants

Plants were grown hydroponically as described by Conn *et al*.,(2013). 1/5 Hoagland's solutions were refilled every 3 days and changed biweekly. Four-week-old plants were subjected to NaCl treatments for an additional 4 weeks for all experiments using hydroponically grown plants unless indicated in the experiment.

Stomatal conductance and CO_2 assimilation rate quantification. Stomatal conductance and CO_2 assimilation rate were measured on the sixth or seventh leaf from the shoot apex. These measurements were made with a LiCor 6400-40 leaf chamber attached to a 6400-XT gas analyzer (LiCor Inc, Lincoln Nebraska). Measurements were taken on the middle portion of the

leaf when the leaf was acclimated to 400-µmol photons m^{-2} s^{-1}, 400 µL L^{-1} CO_2 at 23° C and an airflow rate of 200 µmol s^{-1} after steady-state photosynthesis rates were attained. Each leaf was measured three times and three biological replicates were used for each treatment.

Flow cytometry analysis. The fifth to sixth leaves from the shoot apex of 8-week-old plants were harvested and immediately kept on ice in a ziplock bag. One to three leaves (100 mg) were coarsely chopped with a razor blade and incubated in 1 ml Galbraith buffer (pH 7.0) containing 45 mM $MgCl_2.6H_2O$, 30 mM sodium citrate (trisodium), 20 mM MOPS (3-LN-morpholino propanesulfonate), 1% Triton-100 (10 mg/ml), 2-ME (Mercaptoethanol) as described in Galbraith, (2009) for 30 minutes before nuclei extraction. Homogenate was filtered through a 40 µm nylon filter to remove tissue debris and was used for the rest of the experiment as described by Galbraith *et al*., 2009. Three independent replicates per treatment were included. Samples were analyzed using a FACScan flow cytometer (BD Biosciences, San Jose, CA) with a 15 mW 488 nm argon-ion laser. The flow cytometer was configured for propidium iodide fluorescence measurements using linear amplification. A total of 15,000 cells per sample were acquired and analyzed in the form of DNA ploidy histograms using Cellquest Pro software (BD Biosciences, San Jose, CA) on a Macintosh G5 workstation (Apple Computer, Cupertino, CA).

Leaf area, leaf temperature, and leaf relative water content measurements. Four-week old plants were further incubated for another four week in 150 mM NaCl and subsequently subjected to quantification of total leaf area and relative water content. Leaves were harvested and fixed on an A4 paper, and scanned with an Epson Perfection V600. Scanned leaf images were analyzed with ImageJ to quantify the total leaf area. To obtain relative water content, freshly harvested leaves were first weighed for fresh weight, then submerged in water for 24 h and weighted again for turgid weight, followed by a 7-day incubation at 37° C for dry weight measurement. The dry weight was recorded when there was no change in weight between 2 consecutive weighting events. Relative water content (RWC) was calculated using the formula: RWC (%) = [(fresh weight - dry weight)/(turgid weight - dry weight)]. Leaf temperature was taken on 4-week old plants using a FLIR thermal camera around 11:30 to 12 pm everyday for 7 days. Leaf temperatures were averaged across all leaves for each plant.

Cross-section imaging and staining. To determine the position of root hair emergence, root tips (from root cap to about 1-2 cm above the root cap) were obtained. The freshly-cut root tips were immediately stained with 0.05% Toluidine blue for 1 min, then washed with deionized water for 2 mins. The stained root tips were directly transferred to microscopic slides, and immersed in glycerol.

To investigate the anatomy of the young roots, mature roots, stem, and leaves in *S. parvula*, we used root regions that were ~1 cm away from the root tips, the 2-5 cm region below the shoot and root junction, the 4th, 5th and 6th internodes from the shoot apex, and the 4th, 5th and 6th leaves from the shoot apex, respectively. Samples for freehand-cut cross-sections were processed as described in rapid preparation of transverse sections of plant roots protocol from Dr. Schiefelbein's lab at University of Michigan (https://sites.lsa.umich.edu/schiefelbein-lab/rapid-preparation-of-transverse-sections-of-plant-roots/) except that we used 2% semi-solidified agarose media to embed the samples. Root and shoot cross-sections were stained with 0.05% Toluidine blue and 0.01% Safranin-O, respectively, for 30 seconds to 1 min, subsequently washed twice with deionized water, and examined with a Leica DM6B Upright Microscope which features a Hamamatsu sCMOS camera in brightfield illumination.

Fixed-plant cross sections of mature roots, stems, and leaves were prepared by fixing tissues overnight at 4°C in glutaraldehyde (2.5%) and formaldehyde (2.0%) in 0.1M phosphate buffer (PB) at pH 7.4. Samples were post-fixed in 1.0% osmium tetroxide in 0.1M PB at pH 7.4 for two hours, later rinsed with deionized water three times for five minutes each, and dehydrated in an ethanol series at room temperature. Samples were infiltrated with a series of Epon resin and embedded in 100% Epon plastic resin. Plastic resin embedded samples were sectioned at a thickness of 0.5 µm and stained in 0.5% toluidine blue O. The cross section images of leaves, mature roots and stems of *S. parvula* were taken at 20x or 10x magnification with an Olympus light microscope (Olympus, IX81 microscope).

A minimum of 5 biological replicates were used for each quantification. All quantifications of anatomical traits were performed with ImageJ (Schneider *et al*., 2012).

Stomatal staining and counts. Leaf blades between the midrib and the leaf margin were

collected from 8 week-old plants that were previously treated for 4 weeks with 150 or 250 mM NaCl. At least three biological replicates were obtained. Small pieces of freshly detached leaves were immersed in 1/10x (w/v) propidium iodine solution for five to ten minutes and imaged on a Confocal Laser Scanning Microscopy (CLSM). Propidium iodide was excited at 535 nm and the emission was collected at 570 to 630 nm. Argon excitation laser (488 nm) was used, and the PI emission color is red. Stomata/unit area was calculated in ImageJ (Schneider *et al*., 2012). We counted the number of stomata on both hydroponically and soil grown plants with the same developmental stage and treatment duration. The leaf epidermis was peeled and positioned on microscopic slides in glycerol and imaged using an Axiovert 200M microscope equipped with Hamamatsu ORCA-ER digital camera.

Scanning micrographs for wax imaging. For scanning electron microscopy, freshly detached *A. thaliana* and *S. parvula* leaves were mounted on the specimen stubs using double-sided tape and observed under high vacuum mode at 5.0 kV in a JEOL JSM 6610LV scanning electron microscope.

Soil grown plants

Plants were grown on soil as described in Wang *et al*., (2019). In brief, dried unsterilized *S. parvula* and *A. thaliana* seeds were sowed directly on pre-moistened soil (Metro Mix 360, Sungro Horticulture, Agawam, MA), stratified at 4°C for 5-7 days, and grown in a growth chamber with a light cycle of 14 h light and 10 h dark, 100-130 umol m^{-2} s^{-1}, and 22-24°C unless indicated otherwise. The plant age and stress treatment strength and duration were specifically mentioned for each experiment in the figure caption.

Flowering time and number of flowers and siliques. 3-week-old plants were treated with an increment of 50 mM NaCl up to 150 mM NaCl every 2 days and maintained at 150 mM NaCl for the remainder of the experiment under 16 hr day/ 8 hr night for long day, 12hr day/12 hr night for short day photoperiod regimes. Flowering time was recorded when the first flower was observed. Total numbers of flowering events, including all developing, mature, and aborted flowers, and successfully developed siliques were counted separately for each plant throughout its lifetime.

Silique area and seed size. Five week-old plants were treated with 150 mM NaCl every 2 days for an additional 2 weeks. We sampled the siliques from the top of the branches to ensure that those siliques were developed from the newly formed flowers after the salt treatment. 4 replicates were used and each replicate included 40 siliques from two plants. Size of the siliques and seeds was quantified with imageJ (Schneider *et al*., 2012).

Gene copy number variation via OrthoNet

The copy numbers and transposition states of PhyB/D orthologs were determined using CLfinder-OrthNet pipeline as described by Oh and Dassanayake (2019).

Results

The defining traits of *Schrenkiella parvula* as an extremophyte should reflect the environmental constraints that have shaped its phenotype and collectively make it distinct from other more stress-sensitive annuals in Brassicaceae, including *Arabidopsis thaliana*. Responses to abiotic stresses in *S. parvula* exist as induced or plastic adaptive traits together with genetically fixed traits that also characterize its lifestyle. Additionally, *S. parvula* shares many traits with the model plant, *A. thaliana*, that make it an excellent model including comparable genome size (Dassanayake *et al*., 2011), similar life cycle duration, self-pollination, and prolific seed production (Table 1 and Fig 1). We do not know which traits contribute more than other traits in a stress-adapted lifestyle this species exemplifies albeit many genetic features can be identified to set it apart from other Brassicaceae species. Therefore, we have assessed stress-induced responses exhibited by *S. parvula* during physiological, structural, and developmental responses to determine which set of key traits are most influential in dynamically adjusting growth to survive environmental stresses primarily tested using salt stress. Additionally, we use fixed genetic phenotypes *S. parvula* shows to identify adaptive traits supported by genomic or transcriptomic features that facilitate its niche-specific lifestyle in an extreme habitat.

***S. parvula* adjusts root growth, structure, and form under high salinity**

S. parvula roots, in contrast to *A. thaliana*, maintained uninterrupted root growth in response to salt stress compared to control conditions (*i.e.* no added NaCl in the growth medium; see Methods) (Fig 2A). Remarkably, *S. parvula* primary root length did not indicate any growth retardation even at longer durations or higher concentrations of salt stress while *A. thaliana* showed growth inhibition at any concentration tested (Fig 2B). While this trend remained the same for lateral root growth, the emergence of lateral roots was delayed in *S. parvula* even at control conditions compared to *A. thaliana* (Fig 2C). Unlike primary or lateral roots, root hair development in *S. parvula* was more sensitive to high salinity; root hairs showed a consistent decrease in length at higher salinities or during longer exposure times to salt stress (Fig 2D and S1). The ability to maintain or enhance primary root growth under high salinity by *S. parvula* was not limited to seedling stages and remained as a consistent trait shown by mature plants even at longer durations and higher salinities tested using 250 mM NaCl in a hydroponic growth medium (Fig S2).

Galvan-Ampudia *et al*. previously reported that *A. thaliana* roots actively avoid salt stress by primary roots bending to grow away from higher salt concentrations when salt was introduced in a gradient salt medium (Galvan-Ampudia *et al*., 2013). We can recapitulate this phenotype in *A. thaliana*. Interestingly, in comparable growth conditions, *S. parvula* showed salt insensitive primary root growth where the root grew into the salt medium without changing its course, further exemplifying its higher tolerance to high salinity (Fig S3).

While root growth responses to salt treatments were apparent within days after exposure to salt, we predicted that longer exposure times in *S. parvula* may not only lead to changes in overall root length but may also result in anatomical adjustments in roots. Therefore, we examined the tissue level structural responses in *S. parvula* roots of 8-week-old plants that had been treated for 4 weeks with 150 mM NaCl (Fig 3). These traits were catalogued from root tips to mature roots (Fig S4).

In young roots, most notably, the length of the root tip that includes the cap and the meristematic and elongation zones was longer (measured as the length from the tip to the first root hair emergence site) under high salinity compared to control conditions (Fig 3B). Although we used 8-week-old plants for this experiment, the young roots in salt treated plants were

produced during the 4-week treatment. We did not observe any anatomical trait adjustments when considering cell type or tissue-layer allocation differences as a response to salinity in young roots of *S. parvula* (Fig 3C). However, *S. parvula* develops two layers of cortical cells in both control and salt-treated samples (Fig S4A).

The structural adjustment shown by mature roots in response to high salinity was distinct from young roots of *S. parvula*. Xylem tissues in mature roots significantly increased in area as a response to high salinity (Fig 3D and S4B). However, this did not affect the overall root diameter. The xylem tissue expansion was primarily caused by increased vessel element size and the extra space taken up by the xylem tissue was compensated by constricting the cortical air spaces (unstructured aerenchyma) in mature roots (Fig 3D and S4B).

S. parvula shoots change in form and function to respond to salt stress

Structural adjustments in response to long-term salt stress extend to shoot tissues in *S. parvula* (Fig 4). Long term salt stress leads to larger vessel elements in *S. parvula* shoots (Fig 4A) keeping a root-shoot continuum with root vessel elements that increase in size when exposed to high salinity (Fig 3D). The expansion in vessel element size in shoots was matched by a reduction in cambial and cortical zones that kept the average shoot area constant between control and salt treated plants (Fig 4A, S5) while other cell or tissue layers in the shoot remained unchanged when treated with salt (Fig S5).

Leaves developed during long-term salt treatments in *S. parvula* showed increased succulence as indicated by increases in the leaf thickness across the leaf including the midrib (Fig 4B and S6). A previous study demonstrated that increased endoreplication induced by salinity can cause cell size expansion and succulence in the salt tolerant plant, *Mesembryanthemum crystallinum* (Barkla *et al*., 2018). We tested whether *S. parvula* shared a similar trait in response to salt by quantifying ploidy of leaf cells. Indeed, the proportion of leaf cells with higher ploidy increased with higher salinities and the endoreplication index increased significantly at 250 mM NaCl treatment compared to the control condition (Fig 4C). *S. parvula* leaves showed both structural and functional adjustments to salt treatments that coincided with its photosynthetic capacity and water use efficiency (Fig 5), but the total leaf number per

plant remained similar between control and salt-treated plants. Salt treatments not only increased leaf succulence, but also leaf area, suggesting a growth-promoting effect at least with the long-term 150 mM NaCl treatment (Fig 5A). Bigger and thicker leaves developed in response to increased salinity suggest that *S. parvula* may demonstrate high water use efficiency under salinity stress.

Leaf shape, angle and phyllotaxis, stomatal distribution, and boundary layer thickness caused by thick cuticles or trichomes largely contribute to efficient use of water by plants (Yoo *et al*., 2009). *S. parvula* leaves are amphistomatous (i.e. presence of stomata on both abaxial and adaxial surfaces), linear-lanceolate with a narrower base, and trichomeless (Table 1, Fig 5A and 5B). Water loss from leaves occurs through stomata and leaf epidermis. In *S. parvula*, stomatal density did not change between control and salt-treated fully-mature leaves that developed during long-term salt treatments (Fig 5B). However, stomatal regulation was adjusted with increasing salinities as indicated by decreased stomatal conductance (Fig 5C) and decreased CO_2 assimilation, notably at much higher salinities for *S. parvula* than observed for *A. thaliana* (Fig 5D). When 100 mM salt treatments were sufficient to cause a drop in both stomatal conductance and photosynthesis in *A. thaliana*, *S. parvula* was able to maintain transpiration (based on stomatal conductance) and photosynthesis (based on the of CO_2 assimilation) to comparable levels measured for plants grown at control conditions and consequently maintained lower average leaf temperatures than *A. thaliana* (Fig 5E). Remarkably, *S. parvula* maintained its relative leaf water content at all tested salinities up to 250 mM NaCl (Fig 5F). This suggests that *S. parvula* optimized effective use of water instead of simply reducing water loss at high salinities. Prioritizing effective water use has been proposed as a better strategy for plant growth during water deficit stress instead of maximizing water conservation at the expense of photosynthetic capacity (Blum, 2009).

Minimized non-stomatal transpiration by enhanced epidermal boundary layer resistance to water loss is equally important as stomatal regulation to achieve effective water use under water stress (Blum, 2009). Indeed, previous findings have demonstrated that *S. parvula* leaves had a significantly thicker leaf cuticle supported by a higher level of total wax content compared to *A. thaliana* leaves (Teusink *et al*., 2002) (Fig S7A). Interestingly, when we

compared the basal expression of key genes in the wax biosynthesis pathway (Rowland *et al*., 2006; Greer *et al*., 2007; Chacón *et al*., 2013; Pascal *et al*., 2019) from comparable shoot tissues grown under control conditions (Oh *et al*., 2014), we see consistently higher constitutive expression in *S. parvula* compared to their ortholog expression in *A. thaliana* (Fig S7B).

Leaf functions are tightly coupled to evaporative cooling enabled by phyllotaxis and leaf form in addition to stomatal regulation and water use efficiency that facilitate active plant growth amidst stressful conditions (Lin *et al*., 2017; Jagadish *et al*., 2021). Although changes to leaf shape and arrangement is not a salt dependent inducible trait in *S. parvula*, it is worth stating that its narrow leaves with elongated petioles arranged spirally on erect stems with elongated internodes (Fig S8A) are ideally suited to rapid growth in saline habitats with warm temperatures where efficient transpirational cooling imparts selective advantages (Lin *et al*., 2017). Additionally, an erect growth habit is more desirable than a rosette to minimize leaf contact with soil, given that *S. parvula* is found near saline lakes with top soils often enriched in salt crystals (Hajiboland *et al*., 2018; Tug *et al*., 2019; IPNI, 2021). Notably, key traits resulting in narrow leaves and elongated petioles and internodes are influenced by the phytochrome family of genes (Somers *et al*., 1991; Li *et al*., 2011). Interestingly, *S. parvula* plants closely resemble the morphology of *A. thaliana phyB phyD* double mutants (Devlin *et al*., 1996; Li *et al*., 2011). Among *A. thaliana PHY* genes, *PHYB* and *PHYD* form a single clade (Li et al., 2011), therefore, we searched for genome level cues for loss of function or altered function in *S. parvula PHY* genes that may support such a phenotype being selected as the only observed and herbarium documented growth form of *S. parvula* (Fig 1 and Table 1) (German and Al-Shehbaz, 2010). We observed that *PHYB* is conserved as a single copy in six closely related Brassicaceae genomes we examined, with a translocation event in lineage I and II species, but *PHYD* appears to have undergone gene loss in *S. parvula* as a lineage specific event (Fig. S8B).

Salt stress induces early flowering and silique formation in *S. parvula*

We examined long-term salt stress responses targeting reproductive traits to investigate how excess Na^+ affected fitness of *S. parvula* (Fig 6). Salt treatments induced early flowering irrespective of whether flowering time was measured as the number of days to detect the first

floral buds after planting or the number of leaves developed before flowering (Fig 6A-C). Additionally, early flowering induced by salt was consistent between long-day and short-day photoperiods (Fig 6C). The initial (~10) flowers produced under control conditions aborted without developing into siliques compared to salt-treated plants (Fig 6A and 6B), suggesting that *S. parvula* favors adding salt beyond tolerance of exposure to salt (at least at concentrations we have tested, which are known to exert salt stress in most plants). *S. parvula* flowers can self-fertilize, and the elongation of filaments that reach the level of the stigma facilitates this process. However, early flowers under control conditions develop shorter filaments than in the salt-treated plants (Fig 6D). This appears to hinder successful fertilization and delay subsequent silique formation in control plants (Fig 6A and 6E). Notably, the salt-induced early flowering and salt-dependent elongation of filaments are not specific to NaCl treatments and can be initiated by KCl at similar concentrations (Supplementary Fig S9). At later reproductive stages, the continuous growth of multiple floral meristems in *S. parvula* leads to fertile flowers even under control conditions. Despite the early success of silique formation in salt treated plants, the cumulative number of flowers and siliques produced by control plants surpasses that of salt-treated plants towards the end of their lifecycle. For example, at 74 days after planting, the control plants have a higher number of flowers per plant than salt-treated plants (Fig 6E). The experiment was discontinued when salt-treated plants stopped producing new inflorescences and were senescing (approximately 74 days after planting). Therefore, *S. parvula* does not require salt to increase fitness and salt treatments appear to only provide a transient advantage at early reproductive stages. Even if fitness is higher for control plants compared to salt-treated plants when evaluated based solely on the total number of siliques produced per plant within the entire lifecycle, there may be additional benefits when seeds develop on plants exposed to long-term high salinity, especially if the seasonal changes at its natural habitats reward a strategy of salt-accelerated reproduction. The average size of siliques and seeds of salt-treated plants increased significantly compared to control plants (Fig 6G-I). This suggests that more resources are available for seeds when produced by salt-treated plants compared to control plants. However, seeds from both treated and control groups do not show differences in the rate of germination in the subsequent generation if germinated on media

without added NaCl.

***S. parvula* seed germination is delayed under high salinity and is sensitive to specific salts**

Past studies have reported that many plants including salt-adapted plants delay or pause germination in saline media even if their seedling stages can tolerate high salinity (Ungar, 1978; Kazachkova *et al*., 2016). Both *S. parvula* and *A. thaliana* show decreased seed germination rates compared to control conditions as NaCl concentrations given to induce salt stress increased (Fig. 7A). However, unlike the more salt tolerant traits *S. parvula* has shown compared to *A. thaliana* during seedling and mature developmental stages (Fig 2 and 4), *S. parvula* seed germination appears to be more sensitive to NaCl than *A. thaliana* seeds (Fig 7A). However, this salt-influenced trait does not lead to a binary outcome between germinated vs ungerminated seeds. The smaller fraction of *S. parvula* seeds that formed a radicle continued to develop in a high salinity medium similarly to those seedlings germinated on control conditions, while *A. thaliana* seeds that formed radicles in a high saline medium did not survive to continue to develop hypocotyls (Fig S10A). Up to 90% of ungerminated *S. parvula* seeds on high saline growth media (*i.e.* no visible radicle emergence) germinated and further developed into seedlings when transferred to control media without added NaCl (Fig S10B). This suggests that NaCl introduces a reversible barrier to germination for *S. parvula*.

The native soils of *S. parvula* ecotype Lake Tuz contain high levels of K, Li, and B salts in addition to Na salts (Tug *et al*., 2019). Therefore, we tested if other salts induced a reversible inhibition to seed germination in *S. parvula* as observed with NaCl. KCl induced a similar inhibitory response as observed with NaCl (Fig 7B and S10), but neither LiCl nor H_3BO_3 induced any germination inhibition in *S. parvula* (Fig 7C-D). Contrastingly, *A. thaliana* seed germination was highly sensitive to high LiCl and H_3BO_3 in the growth medium and high KCl was lethal to *A. thaliana* seeds that formed a radicle at 150 or 250 mM KCl (Fig 7C-D and S10A). This suggests that *S. parvula* is adapted to sense the salt level as well as the salt type before radicle emergence and if seeds germinate, they are more likely to continue growth despite the toxic levels of salts in the growth medium that is lethal to *A. thaliana*.

Salt-dependent germination of *S. parvula* suggests that it is an adaptive trait to time seed germination when soil salinity of the topsoil layer decreases during summer months from June to September. This is supported by field observations made in the Lake Tuz region where *S. parvula* grows as a seasonal annual during the months that receive the highest rainfall and temperature with the longest day length than the rest of the year (Fig S11A, B and C). The saline soils surrounding Lake Tuz are often covered with a salt crust towards mid-summer, which becomes a dominant feature in the landscape extended to spring of the following year despite having a high saline water table throughout the year (Tug *et al*., 2019). Given that seed germination may range widely within the expected growing season and seedlings are more vulnerable to extreme environmental conditions than mature plants, we tested the thermal tolerance of *S. parvula* compared to *A. thaliana* subjected to heat, chilling, and freezing stresses to assess how it may fit within the expected temperature tolerance range required to survive in its native habitat (Fig S11D,E and F). *S. parvula* seedlings showed much higher tolerance to heat stress given at 38°C compared to *A. thaliana* (Fig S11F), while chilling and freezing tolerance in both species seemed equivalent (Fig S11D and E).

Discussion

Plants are known for their remarkable capacity to tolerate environmental stresses and when possible escape stress by modulating growth even up to levels where growth is completely paused. This plasticity to respond to various environmental stresses is observed in all plants, and extremophytes such as *S. parvula* have a much higher tolerance than glycophytes such as most crops and *A. thaliana,* in agreement with our current study (Flowers and Colmer, 2008; Kazachkova *et al*., 2018). About 40% of all halophytes (although halophytes represent only about 0.4% of all flowering plants) are able to withstand salt stress even at concentrations similar to seawater (Kotula *et al*., 2020). At high salinities, all plants respond to salt stress by inhibiting growth to prioritize survival as a tradeoff (Santiago-Rosario *et al*., 2021). Nevertheless, the extremophyte model *S. parvula* provides a genetic system to discover adaptive traits that do not show a growth compromise at salt concentrations (known to be lethal to most crops and *A. thaliana* (Oh *et al*., 2014). When we examine its physiological and structural traits that change at a developmental-stage-specific and tissue-specific scale in

response to salt stress, we see several traits that emerge as significant features induced under salt stress compared to their control group (Fig 8A). Among them, the higher number of siliques produced during salt induced early flowering, expansion of xylem vessel elements, and increased leaf thickness contribute the most to the total plastic or inducible trait space more than other traits that change significantly between salt-treated and control growth conditions (Fig 8B and C). In the following sections we discuss the significance of the most impacted traits serving adaptive roles characterizing the extremophytic lifestyle of *S. parvula*.

Salt stress aids in maximizing fitness of *S. parvula* by accelerating the transition to a reproductive stage from an exclusive vegetative growth phase

Salinity is known to delay flowering in most plants (Blits and Gallagher, 1991; Lutts *et al*., 1995; Apse *et al*., 1999; Moriuchi *et al*., 2016; Cho *et al*., 2017). For example, high salinity (≥100 mM NaCl) delays or inhibits the transition from vegetative to reproductive growth in *A. thaliana* (Achard *et al*., 2006; Li *et al*., 2007; Ryu *et al*., 2014). It is widely accepted that delayed flowering ensures increased survival under salt stress supported by multiple genetic mechanisms. These pathways include transcription factors that are known to inhibit flowering and are also induced by salt (Cho *et al*., 2017). However, a few plants have been reported to show alternative strategies of salt-accelerated flowering (Adams *et al*., 1998; Ventura *et al*., 2014) despite the risk of death due to adverse effects of prolonged salt stress. Additionally, molecular pathways operating antagonistically to salt-induced delayed-flowering have been described for *A. thaliana* (Yu *et al*., 2018). This apparently riskier strategy would facilitate reproduction and improve fitness by allowing escape from harsh environments, especially for ruderal or annual plants growing in habitats that become warmer, drier, and more saline (due to increased surface evaporation) towards the end of their growing season. Salt-induced flowering observed for *S. parvula* suggests that such an alternative strategy was selected as the dominant trait to maximize its fitness in its native habitat exemplified by the Lake Tuz ecotype used in our current study (Fig 6, S9) over the more common trait of salt-induced delay in flowering observed for many other plants.

Compared to growth favorable conditions, environmental stresses increase the opportunity for selection. Previous studies have demonstrated that phenotypic selection favored stress-avoidance traits, including earlier flowering, compared to stress-tolerance traits. This results in an evolutionary shift toward earlier flowering despite the prevalent trait observed for model and crop plants to delay flowering when exposed to salt (Stanton *et al*., 2000; Ventura *et al*., 2014; Caño *et al*., 2016; Moriuchi *et al*., 2016). Stanton *et al*., (2000) further showed that the potential for selection was greatest for high salt stress (in addition to low light) among multiple environmental stresses tested, including low nutrient and drought, for their effects in evolutionary selection on wild mustard, *Sinapis arvensis* (a ruderal annual in Brassicaceae). *S. parvula* is native to the variable shoreline habitats of saline lakes in the Irano-Turanian region where it is often a ruderal plant growing in frequently inundated saline soils (Ozfidan-Konakci *et al*., 2015; Hajiboland *et al*., 2018; Tug *et al*., 2019). Therefore, salt stress is the norm for *S. parvula* and over generational times salt stress is expected to provide a constant selection pressure in defining its lifestyle.

Most studies exploring salt stress responses focus on vegetative growth phases, but when we examined salt-responsive traits throughout the lifecycle of *S. parvula*, increased number of siliques produced due to early flowering induced by salt stress had the largest fold-change among other salt induced traits that differentiate the response between control and salt-treated growth (Fig 8C). While early flowering established earlier seed set and opportunity to produce viable seeds in an earlier developmental age in the salt treated plants compared to control plants (Fig 6), this is a plastic trait not necessarily imparting higher fitness assessed based on overall fecundity (i.e. the total number of seeds produced per plant in its entire lifecycle) in salt vs control conditions if plants continued to grow past 2 months. The control plants showed longer vegetative growth phases subsequently leading to higher fecundity in *S. parvula.* These results suggest that salt-induced flowering has evolved as a mechanism of stress avoidance rather than stress tolerance in a habitat where the severity of environmental stresses increase as the growing season extends (Fig S11).

A key morphological feature contributing to the transient advantage of early flowering is the plastic response observed for filament elongation enhanced by salt in *S. parvula* (Fig 6D, S9). Early flowers between salt-treated and control conditions differ in growth rates of filament elongation, a trait that is important for successful fertilization in selfing plants such as *S. parvula* and *A. thaliana*. Additionally, salt stress is known to terminally inhibit gamete formation, and lead to abortion of flowers and seeds (Sun *et al*., 2005), and several genetic pathways regulating stamen growth influenced by salt stress are described for *A. thaliana* (Bassil *et al*., 2011; Monihan *et al*., 2016). Filament elongation and production of viable seeds are not inhibited by salt in *S. parvula*, in contrast to the inhibition of these traits seen in *A. thaliana* (Fig 6), indicating that *S. parvula* has evolved to decouple the regulatory pathways that sense salt and inhibit stamen growth.

Xylem vessel expansion across the root-shoot continuum induced by salt observed in the stress resilient growth of *S. parvula*

Selection on vessel diameter favors narrower vessels to minimize the risk of cavitation independently of ancestry or habitat for a wide range of angiosperms from rainforests to deserts (Olson and Rosell, 2013). Furthermore, the effect of salt stress on xylem development within a species often leads to narrower vessels (Junghans *et al*., 2006; Ge *et al*., 2017; Cruz *et al*., 2019; Sarker and Oba, 2020). Our results suggest an alternative strategy for *S. parvula* where xylem vessel diameter increases when plants were exposed to long-term salt stress (given via 150 mM NaCl) both in roots and shoots (Fig 3 and 4). The expansion of xylem tissue in *S. parvula* induced by salt stress is the second most highly impacted trait that responds at a higher fold change between control and salt-treated plants (Fig 8). This adaptive feature, although adds a tradeoff of a higher risk for cavitation during salt stress, seems to allow a higher bulk flow through the xylem that helps *S. parvula* leaves maintain a cooler temperature while allowing uninterrupted gas exchange compared to control conditions and to *A. thaliana* grown in comparable conditions (Fig 5). Salt-induced increases to xylem diameter promoting growth under salt stress have been reported for a few extremophytes (e.g. *Nitraria retusa* and *Atriplex halimus*) adapted to extreme salinities above seawater strength, but is not a common trait associated with halophytes (Boughalleb *et al*., 2009; Parida *et al*., 2016). The expansion of

xylem area without the allocation of resources to expand the root or stem diameter observed as a salt responsive trait in *S. parvula* is an atypical adaptation among plants to promote growth while being resilient to salt stress (Olson and Rosell, 2013; Nassar *et al*., 2020). If availability of water can be ensured in agricultural systems even if the water source is brackish, crops that are able to maintain their relative water content within the plant to levels seen in growth optimal conditions (as observed for *S. parvula* in Fig 5), while allowing uninterrupted transpiration and gas exchange, will serve as better crops resilient to environmental stresses.

Adjustments to shoot architecture modulation follows root responses to cope with salt stress

The growth strategy exemplified by *S. parvula* for promoting growth dependent on modulating root to shoot vasculature seemed to be efficiently coupled with leaf traits in *S. parvula*. Even though salt stress when it exists as an edaphic factor directly affects roots, its effects are seen also in shoots. If roots grow in continuous saline media, salts are often deposited in leaves and, as plant ages, salt adapted plants either need to store salts in leaves and shed leaves that can no longer serve to compartmentalize excess salt, or to extrude via salt glands (Jennings, 1968; Dassanayake and Larkin, 2017). *S. parvula* uses the first strategy by developing succulent leaves that can store excess salts and this trait is facilitated by shifting the leaf cell population from a dominant diploid state to higher ploidy levels during prolonged salt stress (Fig 4). Consequently, the increase in leaf thickness, along with larger leaf area, is among the top salt-induced traits in *S. parvula* (Fig 8). Developing larger cells that can store excess salts with larger vacuoles enabled by endoreplication has been reported for several other salt adapted extremophytes proposed as a key mechanism to survive environmental stress (De Rocher *et al*., 1990; Barkla *et al*., 2018), while leaf succulence is one of the most common traits observed in halophytes (Jennings, 1968; Flowers and Colmer, 2008).

To maximize storage capacity via increasing the leaf surface area to volume, leaves are generally more terete in many extremophytes that have fully developed succulent leaves. This trait is often accompanied by losing the abaxial identity of the leaves where leaves become adaxialized (Ogburn and Edwards, 2013). Multiple genetic networks regulated by adaxially

expressed HD-ZIPIII transcription factors have been shown to control leaf polarity (Du *et al*., 2018). *S. parvula* leaves tend to acquire a more terete state with prolonged exposure to salt (Fig S6B). This phenotypic change is coincident with *S. parvula* leaves exhibiting reduced differentiation between adaxial and abaxial surfaces as leaf thickness increases with higher salt concentrations and a clear palisade layer at the adaxial surface is not present. However, this structural alteration does not affect the relative water content nor cause leaf curling or other visibly malformed vascular structures, as seen in adaxialized leaves of *A. thaliana* mutants (Fig 4, 5, and S6, Du *et al*. 2018).

In contrast to the leaves of *A. thaliana*, which have more stomata on the abaxial surface (hyposomatous), *S. parvula* leaves are amphistomatous (Fig 5B). Amphistomatous leaves are relatively rare in angiosperms (Nadeau and Sack, 2002; Drake *et al*., 2019). In amphistomatous leaves the distance between stomata and mesophyll is reduced allowing greater water-use efficiency due to increased CO_2 conductance in the mesophyll and thereby allowing higher relative photosynthesis rates (de Boer *et al*., 2016). Therefore, amphistomatous leaves are found in highly productive fast growing herbs, but when this trait is shown by extremophytes such as *S. parvula* with trichomeless leaves arranged mostly with vertical leaf angles (Fig 1), it adds a higher risk for greater loss of water through transpiration and higher exposure to radiation heat (Drake *et al*., 2019). Drake *et al*., in their review on the evolution of amphistomatous leaves, hypothesize that in thick amphistomatous leaves, vein length per unit leaf area must be larger than hypostomatous leaves of same thickness to avoid desiccation (Drake *et al*., 2019). This would need to be accompanied by additional traits to facilitate the increase in transpirational flow via xylem development from root to shoot if leaf thickness increases as a response to salt stress. Additionally, having mostly vertical leaf angles when thick amphistomatous leaves are present is considered a key adaptive trait to reduce radiation heat around midday while maximizing photosynthesis in the morning and late afternoon with lower risks for desiccation (King, 1997). Further, traits known to have evolved under shade avoidance such as internode elongation seems to be exapted in *S. parvula*, likely to enhance transpirational cooling selected under environments that demand rapid growth amidst extreme environmental constraints (Pierik and Testerink, 2014).

Moderate to high salt is a persistent edaphic factor in the natural habitat of *S. parvula* (Helvaci *et al*., 2004; Tug *et al*., 2019). Such an environment would have selected for multiple traits that act synergistically to create an efficient lifestyle to survive stress. However, unlike many extremophytes *S. parvula* has epitomized efficient growth achieved with short life cycles, while enduring multiple environmental stresses, over slow growth coupled to long life cycles. Often environmental stress resilience comes at the cost of yield reduction in crops and the drive for increasing yields has been prioritized over the need to develop resilient crops (Pardo and VanBuren, 2021). Increasing threats to global agriculture due to climate change necessitate a change in our priorities for crop development (IPCC, 2021). *S. parvula* provides an excellent genetic model system that illustrates growth optimization over growth inhibition to cope with environmental stresses that we can explore to find innovative genetic architecture suitable and transferable to develop resilient crops.

Main figure and table captions

Figure 1. Life cycle of *S. parvula* from seeds to siliques. All scale bars are 1cm unless indicated in the figure.

Table 1. Morphological comparison between *S. parvula* and *A. thaliana*

Figure 2. Effects of NaCl stress on root growth in *S. parvula* and *A. thaliana* seedlings. [A] 12-day-old seedlings of *A. thaliana* and *S. parvula* were grown for 5 days on 1/4 Murashige and Skoog media, and 7 days on indicated concentrations of NaCl. Plates were scanned 7 days after treatment (DAT). [B] Primary root growth, [C] number of lateral roots and lateral root density, and [D] average length of 10 longest root hairs of *S. parvula* and *A. thaliana* seedlings. Asterisks indicate significant changes ($p \leq 0.05$) between the treated samples and its respective control samples, determined by Student's t-test. Data are represented as the mean of 3 independent replicates ± SD (≥ 3 plants per replicate). Open circles indicate the number of plants used for each experiment.

Figure 3. Effects of NaCl stress on *S. parvula* root structures. [A] The position of the transverse sections on the *S. parvula* root. Measurements from [B] root tip, [C] young root, and [D] mature root from 12-week-old hydroponically grown *S. parvula* plants. 8-week-old *S. parvula* plants

were grown under control or 150 mM NaCl conditions for an additional 4 weeks. A minimum of 20 sections from the mature roots of 4-13 plants were used for mature root quantifications for each condition. 5-10 plants were used for young root quantifications under each condition. Asterisks indicate significant changes ($p \leq 0.05$) between the treated samples and its respective control samples, determined by Student's t-test. Data points represent individual cross-sections and colors represent individual plants. Scale bar represents 100 µm.

Figure 4. Effects of NaCl stress on *S. parvula* shoot structures. Transverse section of [A] stem and [B] leaf of 12-week-old hydroponically grown *S. parvula* plants. 8-week-old *S. parvula* plants were grown under control or 150 mM NaCl conditions for an additional 4 weeks. A total of 23 sections from 7 control plants and 32 sections from 9 treated plants were used for leaf measurements, a minimum of 20 sections from 5-11 plants were used for stem measurements. Data points represent individual cross-sections and colors represent individual plants. [C] Nucleus DNA content, distribution of leaf cell ploidy, and endoreplication index of leaf cells from control and 250 mM NaCl-treated 8-week-old S. parvula plants. Data are represented as means of 4 independent replicates taken from 10th and 11th leaves from the shoot meristem. Asterisks indicate significant changes ($p \leq 0.05$) between the treated samples and its respective control samples, determined by Student's t-test. Scale bars represent 100 µm.

Figure 5. Effects of NaCl stress on *S. parvula* leaves. [A] Total photosynthetic leaf area. [B] Stomatal density. [C] Stomatal conductance. [D] Photosynthesis rate. [E] Leaf surface temperature. [F] Leaf relative water content. All experiments were performed with 4-week-old hydroponically grown plants that were treated for an additional 4 weeks with indicated NaCl concentrations. Asterisks indicate significant changes ($p \leq 0.05$) between the treated samples and its respective control samples, determined by Student's t-test. Data are represented as mean of at least 3 independent replicates ± SD. Open circles indicate the number of plants (in B, F, and G) and leaves (in C and D) for each experiment. DAT, days after treatment.

Figure 6. Effects of NaCl stress on fitness of *S. parvula*. [A] Plants grown under control conditions generally flower at ~17th leaf stage and the first few flowers are subsequently aborted. [B] Salt treated plants flower earlier at ~14th leaf stage and the first flowers develop into mature siliques. [C] Days from planting to the first observed flower of plants grown in long

day (16 h light/8 h dark) and short day (12 h light/12 h dark). [D] Filament length in flowers obtained from control and treated plants. [E] Number of flowers and siliques per plant under control and treatment conditions. Open circles represent 4 biological replicates (n=5 plants per replicate). [F] Ratio between the number of flowers and siliques observed for control (C) and salt-treated (T) plants used in D. [G and H] Comparison of silique size from plants under control and NaCl stress conditions. Open circles represent 20 siliques from 10 plants. [I] Comparison of the area of seeds from plants under control and NaCl stress conditions. Open circles represent 50 seeds per treatment from 15-50 plants. For panel [B], the treatment started 21 DAP, initially at 50 mM, included in the water given every other day. The salt concentration increased by 50 mM every four days until reaching 200 mM; for panel [C,E,F], the treatment started on 3-week-old plants until the end of the experiment; for panel [G,H,I], the treatment started on 5-week-old plants, treated for additional 2 weeks. Different letters or asterisks represent significant differences (*, $p < 0.05$) compared to control, determined by either one-way ANOVA followed by either one-way ANOVA followed by Tukey's post-hoc tests [C] or Student's t-test [E, H, I]. DAP, days after planting.

Figure 7. Effects of toxic levels of salts on the germination of *S. parvula* and *A. thaliana* seeds. [A] NaCl, [B] KCl, [C] LiCl, and [D] H3BO3. The germination was recorded three days after planting. Different letters indicate significant differences ($p \leq 0.05$) determined by one-way ANOVA with post-hoc Tukey's test. Data are represented as mean of 4 independent replicates ± SD (50 seeds per replicate). Open circles indicate the biological replicates.

Figure 8. Salt stress induced structural and physiological changes in *S. parvula*. [A] Salt stress induced fold changes of traits quantified in the current study. Asterisk represents significant differences (*, $p < 0.05$) compared to control determined by Student's t-test. [B] and [C] PCA biplot of traits quantified for *S. parvula* under control and salt-stressed conditions in current study. [B] Anatomical traits quantified: LT, Leaf thickness; MT, Midrib thickness; XS, Xylem/stem area; SVA, Area per stem vessel; CbS, Cambium zone/stem area; CtS, Cortex/stem area; XR, xylem/root area; RVA, Area per root vessel; VN, # vessel/root diameter; AS, Air space/root area; YRA, Young root area; CT, Cortical thickness; YRD, Young root diameter; DRH, Root tip to 1st root hair, [C] Physiological traits quantified: AbS, Abaxial stomatal density; AdS, Adaxial

stomatal density; LA, leaf area; SLA, silique area; SA, seed area; PRL, primary root length; LRD, lateral root density; RWC, relative water content; CA, CO2 assimilation; SC, stomatal conductance; RHL, root hair length; NF, number of flowers; NS, number of siliques. DAT, days after treatment; DAP, days after planting.

Supplement figure and table captions

Figure S1. Effects of NaCl stress on root hair growth in *S. parvula* and *A. thaliana*. White arrows indicate root tip positions when the 5-day-old seedlings were transferred to the indicated concentration of salt plates. Note that the marked root positions in *A. thaliana* control and *S. parvula* were not presented in the shown images because the marked regions were out of frame when we captured the root tip region. Scale bars are 0.5 mm. DAT, Days after treatment.

Figure S2. Long term effects of NaCl stress on the root growth of *S. parvula*. [A] Root fresh weight and [B] primary root length of 12-week-old hydroponically grown *S. parvula* plants. 4-week-old plants were subjected to 150 mM NaCl for additional 4 weeks and the treatment was continued or elevated to 250 mM NaCl for another 4 weeks. The plants were grown at 100-150 µmol m-2s-1 photosynthetic photon flux density with a 12/12-h photoperiod. Asterisks indicate significant changes ($p \leq 0.05$) between the treated samples and its respective control samples, determined by Student's t-test. Data are represented as the mean of 9 biological replicates ± SD. For each plot, open circles indicate the number of biological replicates used for each experiment.

Figure S3. Root bending assay at 200 mM NaCl for *S. parvula* and *A. thaliana*. The blue lines indicate the position of seeds. The yellow line marks the separation between ¼ MS media with 0 mM (top) and 200 mM NaCl (bottom). The root bending angle is indicated in curved white lines. g, gravity axis.

Figure S4. Root structures of *S. parvula*. [A] Transverse section of the young root taken at 1-3 cm from the root tip. [1] Young root area; [2] root diameter; [3] epidermis thickness; [4] cortical layer thickness; [5] endodermis thickness. [B] Transverse section of the mature root taken between 2-5 cm below the root-shoot junction. [1] Mature root area; [2] xylem/root area; [3] Area per root vessel; [4] # vessel/root diameter; [5] Air space/root area.

Figure S5. Stem structures of *S. parvula*. [A] Transverse section of *S. parvula* stem (between 4th, 5th, and 6th internodes from the shoot meristem) with cell layers marked in yellow lines for trait quantification. [B] Measurements for stem anatomical features indicated in A. A minimum of 20 sections from 5-11 plants were used for each measurement. Asterisks indicate significant changes ($p \leq 0.05$) between the treated samples and its respective control samples, determined by Student's t-test. Data points represent individual cross-sections and colors represent individual plants.

Figure S6. Leaf structures of *S. parvula*. [A] Transverse section of *S. parvula* leaves. [1] leaf thickness, [2] midrib thickness. [B] Transverse sections of *S. parvula* leaves treated with indicated concentration of salts. All sections come from the 5th or 6th leaf from the root-shoot junction in 8-week-old plants that were treated for 4 weeks.

Figure S7. Leaf surface and the basal expression of genes involved in wax biosynthesis in *S. parvula* and *A. thaliana*. [A] Scanning electron micrographs contrasting *A. thaliana* and *S. parvula* leaf surfaces. [B] Wax biosynthesis pathway and [C] wax biosynthesizing gene that were significantly differently expressed between *S. parvula* and *A. thaliana* at basal level (Oh *et al*., 2014).

Figure S8. Potential genomic clues for the elongated internode and petiole in *S. parvula*. [A] Elongated internode and leaf petiole in *S. parvula* compared to *A. thaliana*. [B] *PhyD* is missing in *S. parvula* genome. OrthNet representing evolutionary histories of orthologous gene groups derived from the six Brassicaceae genomes used in Oh and Dassanayake, 2019. Nodes are color-coded according to the species. Edges show properties either co-linear (*cl*) or transposed (*tr*).

Figure S9. Effects of KCl stress on the fitness of *S. parvula*. [A] Plants grown under control conditions generally flower late and the first few flowers are subsequently aborted. KCl treated plants flower earlier and the first flowers develop into mature siliques. [B] Early flowers in KCl treated plants develop longer filaments compared to control plants. DAP, days after planting.

Figure S10. [A] *S. parvula* (*Sp*) and *A. thaliana* (*At*) seed germination and growth on NaCl and KCl plates. Scale bars are 2 cm. [B] Growth of ungerminated *S. parvula* seeds treated with different concentrations of NaCl (as shown in Figure 7) after transferring to control MS medium.

Figure S11. Climate in the Lake Tuz region. [A] Lake Tuz location from Google Earth. [B] Precipitation and temperature recorded in Konya, Turkey. S. parvula life cycle is from April/May to August/September (Tug *et al*., 2019) (NOAA, 2019). Bars indicate precipitation and lines represent temperature in each plot. [C] Average day length recorded in Konya per month. Red line indicated the day length used for plant growth in the lab setting. [D-F] Survival rate of *S. parvula* under [D] freezing stress, [E] chilling stress, and [F] heat stress compared to *A. thaliana*. 5-day-old seedlings were subjected to temperature treatments and data were recorded 5 days after recovery. Asterisks indicate significant changes between the treated samples to its respective control samples using t-test with $p \leq 0.05$. Data are represented as mean of 4 independent replicates ± SD (n = 3-6 plants per replicate). Open circles indicate the biological replicates.

Acknowledgement

This work was supported by the US National Science Foundation awards MCB-1616827, IOS-EDGE-1923589, US Department of Energy BER-DE-SC0020358, and the Next-Generation BioGreen21 Program of Republic of Korea (PJ01317301) awards. Graduate students KT, GW, PP, and CW were supported by an Economic Development Assistantship and undergraduate students JJ and MG were supported by the President's Future Leaders in Research Program at Louisiana State University (LSU). We acknowledge the productive discussions led by Drs. Hans Bohnert and John Cheeseman at the University of Illinois at Urbana-Champaign (UIUC) that prompted us to initiate this study. We thank the LSU High Performance Computing facility for providing computational resources. We also thank Dr. Ying Xiao in the Shared Instrumentation Facility at LSU for assistance with microscopy imaging. DH thanks undergraduate students Stephanie Presedo at LSU and Rebekah Munaretto, Michael Pettineo, and Aditya Ravindra at UIUC for assisting research on salt-responsive flowering and silique development phenotypes.

References

Achard P, Cheng H, De Grauwe L, Decat J, Schoutteten H, Moritz T, Van Der Straeten D, Peng J, Harberd NP (2006) Integration of plant responses to environmentally activated

phytohormonal signals. Science (80-) **311**: 91–94

Adams P, Nelson DE, Yamada S, Wendy C, Jensen RG, Bohnert HJ, Griffiths H (1998) Tansley Review No. 97 Growth and development of *Mesembryanthemum crystallinum* (Aizoaceae). Genet Breed 171–190

Ali A, Khan IU, Jan M, Khan HA, Hussain S, Nisar M, Chung WS, Yun D-J (2018) The High-Affinity Potassium Transporter EpHKT1;2 From the Extremophile *Eutrema parvula* Mediates Salt Tolerance. Front Plant Sci. doi: 10.3389/fpls.2018.01108

Ali A, Yun DJ (2017) Salt stress tolerance; what do we learn from halophytes? J Plant Biol **60**: 431–439

Apse MP, Aharon GS, Snedden WA, Blumwald E (1999) Salt Tolerance Conferred by Overexpression of a Vacuolar Na+/H+ Antiport in Arabidopsis. Science (80-) **285**: 1256–1258

Barkla BJ, Rhodes T, Tran KNT, Wijesinghege C, Larkin JC, Dassanayake M (2018) Making epidermal bladder cells bigger: Developmental-and salinity-induced endopolyploidy in a model halophyte. Plant Physiol **177**: 615–632

Barros NLF, Marques DN, Tadaiesky LBA, de Souza CRB (2021) Halophytes and other molecular strategies for the generation of salt-tolerant crops. Plant Physiol Biochem. doi: 10.1016/j.plaphy.2021.03.028

Bassil E, Tajima H, Liang Y-CY-C, Ohto MM -a., Ushijima K, Nakano R, Esumi T, Coku A, Belmonte M, Blumwald E (2011) The Arabidopsis Na+/H+ Antiporters NHX1 and NHX2 Control Vacuolar pH and K+ Homeostasis to Regulate Growth, Flower Development, and Reproduction. Plant Cell **23**: 3482–3497

Basso B, Antle J (2020) Digital agriculture to design sustainable. Nat Sustain **3**: 254–256

Bechtold U (2018) Plant Life in Extreme Environments : How Do You Improve Drought Tolerance ? **9**: 1–8

Blits KC, Gallagher JL (1991) Morphological and physiological responses to increased salinity in marsh and dune ecotypes of *Sporobolus virginicus* (L.) Kunth. Oecologia **87**: 330–335

Blum A (2009) Effective use of water (EUW) and not water-use efficiency (WUE) is the target of crop yield improvement under drought stress. F Crop Res **112**: 119–123

de Boer HJ, Drake PL, Wendt E, Price CA, Schulze ED, Turner NC, Nicolle D, Veneklaas EJ (2016) Apparent overinvestment in leaf venation relaxes leaf morphological constraints on photosynthesis in arid habitats. Plant Physiol **172**: 2286–2299

Boughalleb F, Denden M, Tiba B Ben (2009) Anatomical changes induced by increasing NaCl salinity in three fodder shrubs, *Nitraria retusa*, *Atriplex halimus* and *Medicago arborea*. Acta Physiol Plant **31**: 947–960

Caño L, Fuertes-Mendizabal T, García-Baquero G, Herrera M, Begoña González-Moro M (2016) Plasticity to salinity and transgenerational effects in the nonnative shrub *Baccharis halimifolia*: Insights into an estuarine invasion. Am J Bot **103**: 808–820

Chacón MG, Fournier AE, Tran F, Dittrich-Domergue F, Pulsifer IP, Domergue F, Rowland O (2013) Identification of amino acids conferring chain length substrate specificities on fatty alcohol-forming reductases FAR5 and FAR8 from *Arabidopsis thaliana*. J Biol Chem **288**: 30345–30355

Cho LH, Yoon J, An G (2017) The control of flowering time by environmental factors. Plant J **90**: 708–719

Conn SJ, Hocking B, Dayod M, Xu B, Athman A, Henderson S, Aukett L, Conn V, Shearer MK, Fuentes S, *et al* (2013) Protocol: Optimising hydroponic growth systems for nutritional and physiological analysis of *Arabidopsis thaliana* and other plants. Plant Methods **9**: 1–11

Cruz MV, Mori GM, Signori-Müller C, da Silva CC, Oh DH, Dassanayake M, Zucchi MI, Oliveira RS, de Souza AP (2019) Local adaptation of a dominant coastal tree to freshwater availability and solar radiation suggested by genomic and ecophysiological approaches. Sci Rep **9**: 1–15

Dassanayake M, Larkin JC (2017) Making Plants Break a Sweat: the Structure, Function, and Evolution of Plant Salt Glands. Front Plant Sci **08**: 406

Dassanayake M, Oh D-H, Haas JSJS, Hernandez A, Hong H, Ali S, Yun DJD-J, Bressan RARA, Zhu JKJ-K, Bohnert HJHJ, *et al* (2011) The genome of the extremophile crucifer *Thellungiella parvula*. Nat Genet **43**: 913–918

Devlin PF, Halliday KJ, Harberd NP, Whitelam GC (1996) The rosette habit of *Arabidopsis thaliana* is dependent upon phytochrome action: novel phytochromes control internode

elongation and flowering time. Plant J **10**: 1127–1134

Drake PL, de Boer HJ, Schymanski SJ, Veneklaas EJ (2019) Two sides to every leaf: water and CO 2 transport in hypostomatous and amphistomatous leaves. New Phytol **222**: 1179–1187

Du F, Guan C, Jiao Y (2018) Molecular Mechanisms of Leaf Morphogenesis. Mol Plant **11**: 1117–1134

Flowers TJ, Colmer TD (2008) Salinity tolerance in halophytes *. New Phytol 945–963

Galbraith DW (2009) Simultaneous flow cytometric quantification of plant nuclear DNA contents over the full range of described angiosperm 2C values. Cytom Part A. doi: 10.1002/cyto.a.20760

Galvan-Ampudia CS, Julkowska MM, Darwish E, Gandullo J, Korver RA, Brunoud G, Haring MA, Munnik T, Vernoux T, Testerink C (2013) Halotropism is a response of plant roots to avoid a saline environment. Curr Biol **23**: 2044–2050

Gao C (2021) ll Genome engineering for crop improvement and future agriculture. Cell **184**: 1621–1635

Ge W, Zhang Y, Sun Z, Li J, Liu G, Ma Y, Gao J (2017) Physiological and anatomical responses of *Phyllostachys vivax* and *Arundinaria fortunei* (Gramineae) under salt stress. Rev Bras Bot **40**: 79–91

German DA, Al-Shehbaz IA (2010) Nomenclatural novelties in miscellaneous Asian Brassicaceae (Cruciferae). Nord J Bot **28**: 646–651

Gómez R, Vicino P, Carrillo N, Lodeyro AF, Gómez R, Vicino P, Carrillo N, Lodeyro AF (2019) Manipulation of oxidative stress responses as a strategy to generate stress-tolerant crops . From damage to signaling to tolerance stress-tolerant crops . From damage to signaling to tolerance. Crit Rev Biotechnol **0**: 1–16

Greer S, Wen M, Bird D, Wu X, Samuels L, Kunst L, Jetter R (2007) The cytochrome P450 enzyme CYP96A15 is the midchain alkane hydroxylase responsible for formation of secondary alcohols and ketones in stem cuticular wax of arabidopsis. Plant Physiol **145**: 653–667

Hajiboland R, Bahrami-Rad S, Akhani H, Poschenrieder C, Bahrami S, Hossein R, Charlotte A

(2018) Salt tolerance mechanisms in three Irano-Turanian Brassicaceae halophytes relatives of *Arabidopsis thaliana*. J Plant Res **0**: 0

Helvaci C, Mordogan H, Çolak M, Gündogan I (2004) Presence and Distribution of Lithium in Borate Deposits and Some Recent Lake Waters of West-Central Turkey. Int Geol Rev **46**: 177–190

IPCC (2021) Climate Change 2021: The Physical Science Basis. Contribution of Working Group I to the Sixth Assessment Report of the Intergovernmental Panel on Climate Change. Cambridge University Press

IPNI (2021) International Plant Names Index. Published on the Internet http://www.ipni.org, The Royal Botanic Gardens, Kew, Harvard University Herbaria & Libraries and Australian National Botanic Gardens. https://www.ipni.org/

Jagadish SVK, Way DA, Sharkey TD (2021) Plant heat stress: Concepts directing future research. Plant Cell Environ 1992–2005

Jarvis DE, Ryu CH, Beilstein MA, Schumaker KS (2014) Distinct roles for SOS1 in the convergent evolution of salt tolerance in *Eutrema salsugineum* and *Schrenkiella parvula*. Mol Biol Evol **31**: 2094–2107

Jennings DH (1968) Halophytes, Succulence and Sodium in Plants—a Unified Theory. New Phytol **67**: 899–911

Junghans U, Polle A, Düchting P, Weiler E, Kuhlman B, Gruber F, Teichmann T (2006) Adaptation to high salinity in poplar involves changes in xylem anatomy and auxin physiology. Plant, Cell Environ **29**: 1519–1531

Kazachkova Y, Eshel G, Pantha P, Cheeseman JM, Dassanayake M (2018) Halophytism : What Have We Learnt From *Arabidopsis thaliana* Relative Model Systems ? **178**: 972–988

Kazachkova Y, Khan A, Acuña T, López-Díaz I, Carrera E, Khozin-Goldberg I, Fait A, Barak S (2016) Salt Induces Features of a Dormancy-Like State in Seeds of *Eutrema (Thellungiella) salsugineum*, a Halophytic Relative of Arabidopsis. Front Plant Sci **7**: 1–18

King DA (1997) The functional significance of leaf angle in Eucalyptus. Aust J Bot **45**: 619–639

Kotula L, Garcia Caparros P, Zörb C, Colmer TD, Flowers TJ (2020) Improving crop salt tolerance using transgenic approaches: An update and physiological analysis. Plant Cell Environ **43**:

2932–2956

Krämer U (2018) Conceptualizing plant systems evolution. Curr Opin Plant Biol **42**: 66–75

Li AJ, Li G, Wang H, Deng XW (2011) Phytochrome Signaling Mechanisms. Arab B. doi: 10.1199/tab.0148

Li K, Wang Y, Han C, Zhang W, Jia H, Li X (2007) GA signaling and CO/FT regulatory module mediate salt-induced late flowering in *Arabidopsis thaliana*. Plant Growth Regul **53**: 195–206

Lin H, Chen Y, Zhang H, Fu P, Fan Z (2017) Stronger cooling effects of transpiration and leaf physical traits of plants from a hot dry habitat than from a hot wet habitat. Funct Ecol **31**: 2202–2211

Lloyd EA, Oreskes N (2018) Climate Change Attribution: When Is It Appropriate to Accept New Methods? Earth's Futur **6**: 311–325

Lutts S, Kinet JM, Bouharmont J (1995) Changes in plant response to NaCl during development of rice (*Oryza sativa* L.) varieties differing in salinity resistance. J Exp Bot **46**: 1843–1852

Monihan SM, Magness CA, Yadegari R, Smith SE, Schumaker KS (2016) Arabidopsis CALCINEURIN B-LIKE10 functions independently of the SOS pathway during reproductive development in saline conditions. Plant Physiol **171**: 369–379

Moriuchi KS, Friesen ML, Cordeiro MA, Badri M, Vu WT, Main BJ, Aouani ME, Nuzhdin S V., Strauss SY, Von Wettberg EJB (2016) Salinity adaptation and the contribution of parental environmental effects in *Medicago truncatula*. PLoS One **11**: 1–19

Nadeau JA, Sack FD (2002) Stomatal Development in Arabidopsis. Arab B **1**: e0066

Nassar RMA, Kamel HA, Ghoniem AE, Alarcón JJ, Sekara A, Ulrichs C, Abdelhamid MT (2020) Physiological and anatomical mechanisms in wheat to cope with salt stress induced by seawater. Plants **9**: 1–15

Ogburn RM, Edwards EJ (2013) Repeated origin of three-dimensional leaf venation releases constraints on the evolution of succulence in plants. Curr Biol **23**: 722–726

Oh D-H, Dassanayake M, Bohnert HJ, Cheeseman JM (2012) Life at the extreme: lessons from the genome. Genome Biol **13**: 241

Oh D-HHD-H, Hong H, Lee SY, Yun D-JD-J, Bohnert HJ, Dassanayake M (2014) Genome

Structures and Transcriptomes Signify Niche Adaptation for the Multiple-Ion-Tolerant Extremophyte *Schrenkiella parvula*. Plant Physiol **164**: 2123–2138

Oh DH, Dassanayake M (2019) Landscape of gene transposition-duplication within the Brassicaceae family. DNA Res. doi: 10.1093/dnares/dsy035

Olson ME, Rosell JA (2013) Vessel diameter-stem diameter scaling across woody angiosperms and the ecological causes of xylem vessel diameter variation. New Phytol **197**: 1204–1213

Orsini F, D'Urzo MP, Inan G, Serra S, Oh D-HH, Mickelbart M V., Consiglio F, Li X, Jeong JC, Yun D-JJ, *et al* (2010) A comparative study of salt tolerance parameters in 11 wild relatives of *Arabidopsis thaliana*. J Exp Bot **61**: 3787–3798

Ozfidan-Konakci C, Uzilday B, Ozgur R, Yildiztugay E, Sekmen AH, Turkan I (2015) Halophytes as a source of salt tolerance genes and mechanisms : a case study for the Salt Lake area , Turkey.

Pantha P, Oh D-H, Longstreth D, Dassanayake M (2021) Living with high potassium: an asset or a hindrance. bioRxiv 2021.07.01.450778

Pardo J, VanBuren R (2021) Evolutionary innovations driving abiotic stress tolerance in C4 grasses and cereals. Plant Cell

Parida AK, Veerabathini SK, Kumari A, Agarwal PK (2016) Physiological, anatomical and metabolic implications of salt tolerance in the halophyte *Salvadora persica* under hydroponic culture condition. Front Plant Sci **7**: 1–18

Pascal S, Bernard A, Deslous P, Gronnier J, Fournier-Goss A, Domergue F, Rowland O, Joubès J (2019) Arabidopsis CER1-LIKE1 functions in a cuticular very-long-chain alkane-forming complex. Plant Physiol **179**: 415–432

Pierik R, Testerink C (2014) The art of being flexible: How to escape from shade, Salt, And drought1. Plant Physiol **166**: 5–22

De Rocher EJ, Harkins KR, Galbraith DW, Bohnert HJ (1990) Developmentally regulated systemic endopolyploidy in succulents with small genomes. Science (80-) **250**: 99–101

Rodell M, Famiglietti JS, Wiese DN, Reager JT, Beaudoing HK (2018) Emerging trends in global freshwater availability. doi: 10.1038/s41586-018-0123-1

Rowland O, Zheng H, Hepworth SR, Lam P, Jetter R, Kunst L (2006) CER4 Encodes an Alcohol-

Forming Fatty Acyl-Coenzyme A Reductase Involved in Cuticular Wax Production in Arabidopsis . Plant Physiol **142**: 866–877

Ryu JY, Lee HJ, Seo PJ, Jung JH, Ahn JH, Park CM (2014) The arabidopsis floral repressor BFT delays flowering by competing with FT for FD binding under high salinity. Mol Plant **7**: 377–387

Santiago-Rosario L, Kyle H, Elderd B, Hart P, Dassanayake M (2021) No Escape: The Influence of Substrate Sodium on Plant Growth and Tissue Sodium Responses. Ecol Evol. doi: 10.22541/au.162081817.72637329/v1

Sarker U, Oba S (2020) The Response of Salinity Stress-Induced A. tricolor to Growth, Anatomy, Physiology, Non-Enzymatic and Enzymatic Antioxidants. Front Plant Sci **11**: 1–14

Schlenker W, Auffhammer M (2018) The cost of a warming climate.

Schneider CA, Rasband WS, Eliceiri KW (2012) NIH Image to ImageJ: 25 years of image analysis. Nat Methods. doi: 10.1038/nmeth.2089

Solis CA, Yong MT, Vinarao R, Jena K, Holford P, Hill C, Chen Z (2020) Back to the Wild : On a Quest for Donors Toward Salinity Tolerant Rice. **11**: 1–14

Somers DE, Sharrock RA, Tepperman JM, Quail PH (1991) The hy3 long hypocotyl mutant of arabidopsis is deficient in phytochrome B. Plant Cell **3**: 1263–1274

Stanton ML, Roy BA, Thiede DA (2000) Evolution in Stressful Environments . I . Phenotypic Variability , Phenotypic Selection , and Response to Selection in Five Distinct Environmental Stresses Author (s): M . L . Stanton , B . A . Roy and D . A . Thiede Published by : Society for the Study. Evolution (N Y) **54**: 93–111

Sun K, Cui Y, Hauser BA (2005) Environmental stress alters genes expression and induces ovule abortion: Reactive oxygen species appear as ovules commit to abort. Planta **222**: 632–642

Teusink RS, Rahman M, Bressan RA, Jenks MA (2002) Cuticular Waxes on *Arabidopsis thaliana* Close Relatives *Thellungiella halophila* and *Thellungiella parvula*. Int J Plant Sci **163**: 309–315

Tug GN, Yaprak AE, Vural M (2019) The Floristical, Ecological, and Syntaxonomical Characteristics of Salt Marshes and Salt Steppes in Turkey. Tasks Veg. Sci. pp 413–446

Ungar IA (1978) Halophyte seed germination. Bot Rev **44**: 233–264

Ventura Y, Myrzabayeva M, Alikulov Z, Omarov R, Khozin-Goldberg I, Sagi M (2014) Effects of salinity on flowering, morphology, biomass accumulation and leaf metabolites in an edible halophyte. AoB Plants. doi: 10.1093/aobpla/plu053

Wang G, Ditusa SF, Oh D, Herrmann AD, Mendoza-cozatl DG, Neill MAO, Smith AP, Dassanayake M (2021) Cross species multi-omics reveals cell wall sequestration and elevated global transcript abundance as mechanisms of boron tolerance in plants. 1985–2000

Wang G, Pantha P, Tran KN, Oh DH, Dassanayake M (2019) Plant growth and agrobacterium-mediated floral-dip transformation of the extremophyte *Schrenkiella parvula*. J Vis Exp **2019**: 1–8

Wang XJ, Hu QJ, Guo XY, Wang K, Ru DF, German DA, Weretilnyk EA, Abbott RJ, Lascoux M, Liu J quan (2018) Demographic expansion and genetic load of the halophyte model plant *Eutrema salsugineum*. Mol Ecol **27**: 2943–2955

WCSP World Checklist of Selected Plant Families (WCSP). Facilitated by the Royal Botanic Gardens, Kew. http://wcsp.science.kew.org

Yoo CY, Pence HE, Hasegawa PM, Mickelbart M V. (2009) Regulation of transpiration to improve crop water use. CRC Crit Rev Plant Sci **28**: 410–431

Yu Y, Wang L, Chen J, Liu Z, Park CM, Xiang F (2018) WRKY71 Acts Antagonistically Against Salt-Delayed Flowering in *Arabidopsis thaliana*. Plant Cell Physiol **59**: 414–422

Zandalinas SI, Fritschi FB, Mittler R (2021) Global Warming , Climate Change , and Environmental Pollution : Recipe for a Multifactorial Stress Combination Disaster Trends in Plant Science. Trends Plant Sci **26**: 588–599

Zhu JK (2015) The Next Top Models. Cell **163**: 18–20

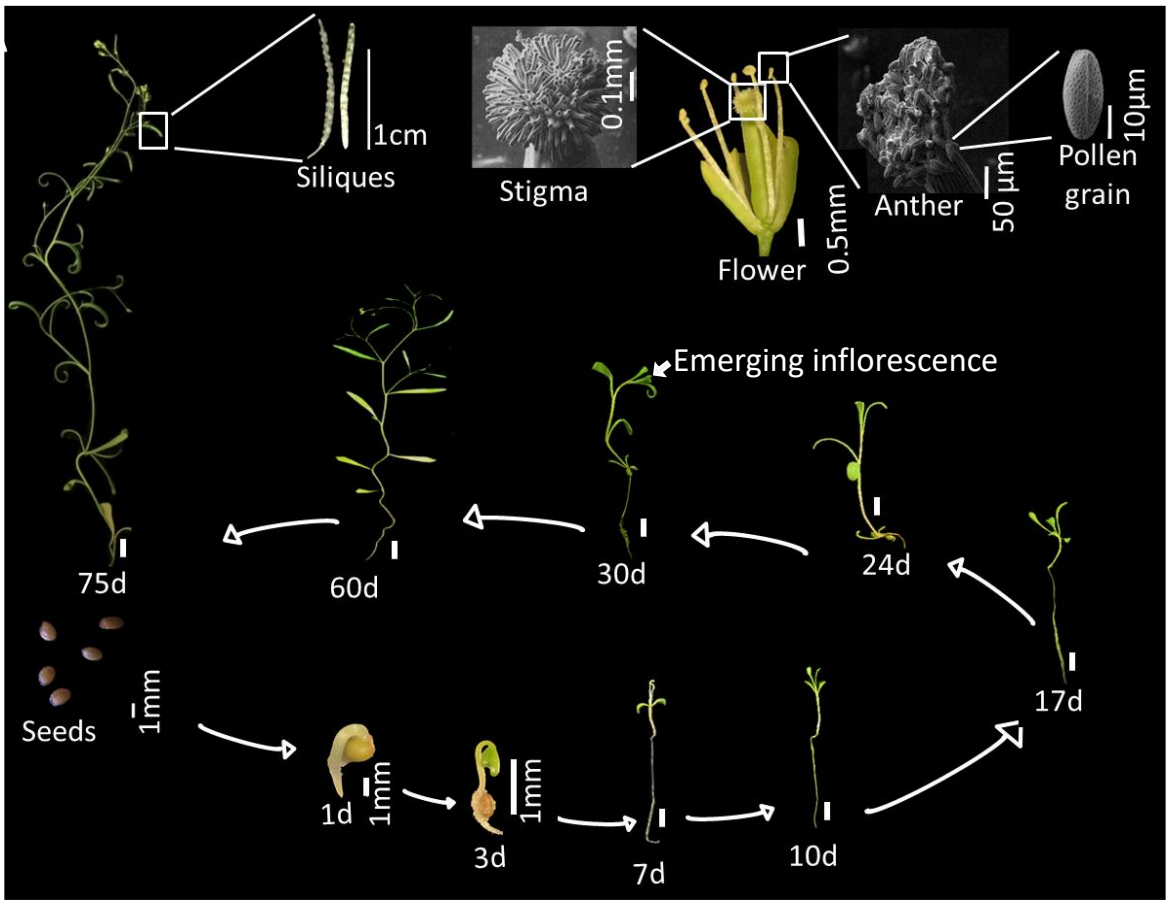

Figure 1. Life cycle of *S. parvula* from seeds to siliques. All scale bars are 1cm unless indicated in the figure**.**

Table 1. Morphological comparison between *S. parvula* and *A. thaliana*

Morphology	*A. thaliana*	*S. parvula*
Growth habit	Determinate	Indeterminate
Leaf arrangement	Rosette	Spiral phyllotaxy
Leaf shape	Ovate	Linear-lanceolate
Trichomes	Present	Absent
Petals	4	Absent
Number of stamens	6 (2 short and 4 long)	6 (equal size)
Siliques/plant[a]	74.9±18.69	61.6±14.40
Silique length (cm)	1.16±0.09	1.48±0.06
Seeds/silique	23.91±13.60	21.58±5.57
Seed weight[b] (g)	0.020±0.003	0.063±0.013
Seed area (mm^2)	0.12±0.02	0.31±0.04

[a] Quantification from 10-12-week-old plants grown under 14-h-day/10-h-night cycle, 22°C - 24°C temperature with a light intensity of 130 µmol m^{-2} s^{-1}.

[b] Average weight of 500 seeds.

Data are represented as mean of 3 independent replicates ± SD.

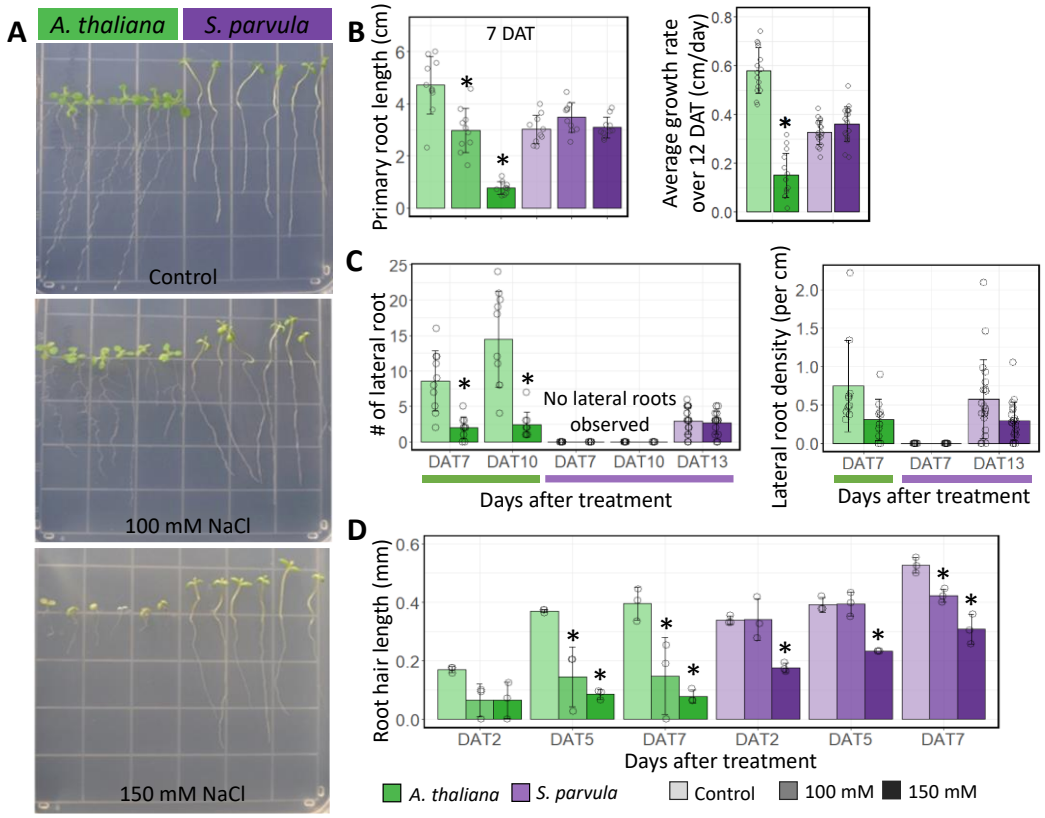

Figure 2. Effects of NaCl stress on root growth in *S. parvula* and *A. thaliana* seedlings. **[A]** 12-day-old seedlings of *A. thaliana* and *S. parvula* were grown for 5 days on 1/4 Murashige and Skoog media, and 7 days on indicated concentrations of NaCl. Plates were scanned 7 days after treatment (DAT). **[B]** Primary root growth, **[C]** number of lateral roots and lateral root density, and **[D]** average length of 10 longest root hair of *S. parvula* and *A. thaliana* seedlings. Asterisks indicate significant changes ($p \leq 0.05$) between the treated samples and its respective control samples, determined by Student's t-test. Data are represented as the mean of 3 independent replicates ± SD (≥ 3 plants per replicate). Open circles indicate the number of plants used for each experiment.

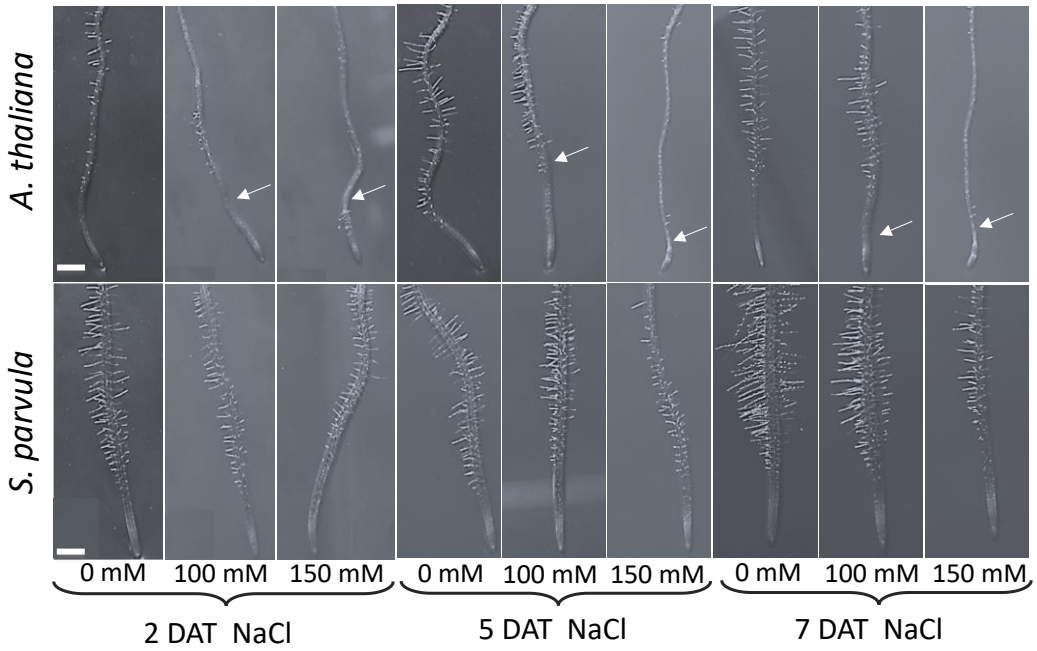

Figure S1. Effects of NaCl stress on root hair growth in *S. parvula* and *A. thaliana*. White arrows indicate root tip positions when the 5-day-old seedlings were transferred to the indicated concentration of salt plates. Note that the marked root positions in *A. thaliana* control and *S. parvula* were not presented in the shown images because the marked regions were out of frame when we captured the root tip region. Scale bars are 0.5 mm. DAT, Days after treatment.

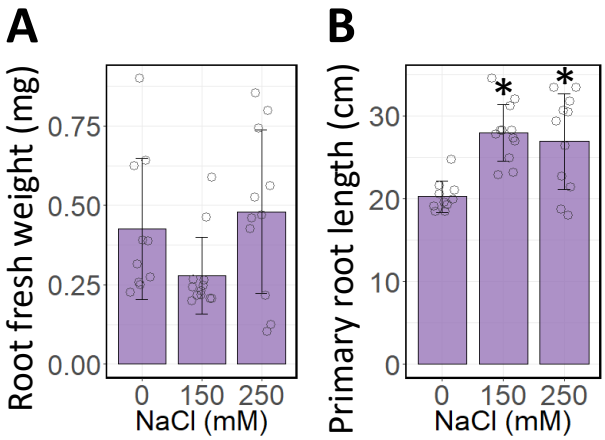

Figure S2. Long term effects of NaCl stress on the root growth of *S. parvula*. **[A]** Root fresh weight and **[B]** primary root length of 12-week-old hydroponically grown *S. parvula* plants. 4-week-old plants were subjected to 150 mM NaCl for additional 4 weeks and the treatment was continued or elevated to 250 mM NaCl for another 4 weeks. The plants were grown at 100-150 µmol m^{-2} s^{-1} photosynthetic photon flux density with a 12/12-h photoperiod. Asterisks indicate significant changes ($p \leq 0.05$) between the treated samples and its respective control samples, determined by Student's t-test. Data are represented as mean of 9 biological replicates ± SD. For each plot, open circles indicate number of biological replicates used for each experiment.

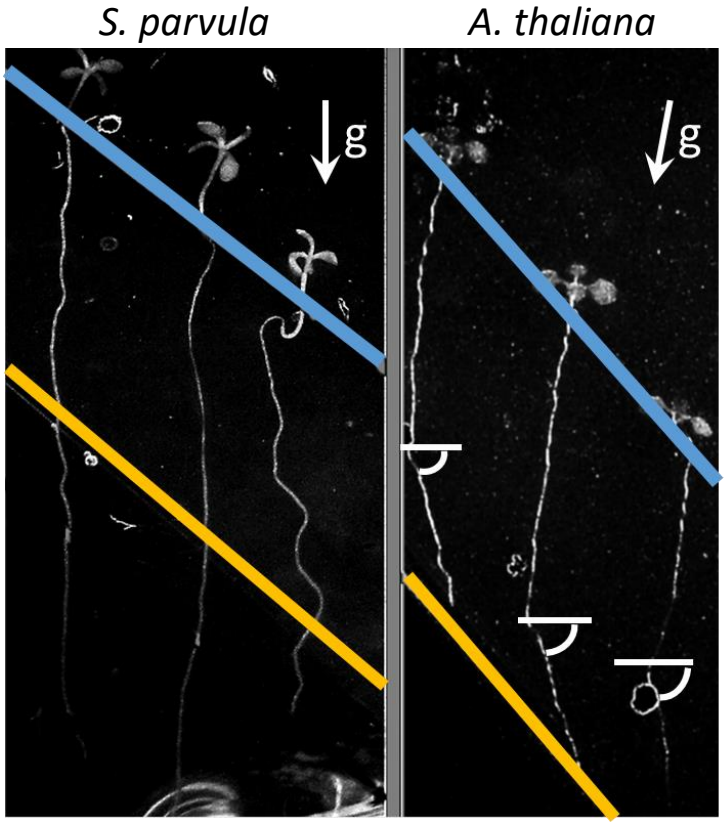

Figure S3. Root bending assay at 200 mM NaCl for *S. parvula* and *A. thaliana.* The blue lines indicate the position of seeds. The yellow line marks the separation between 1/2 MS media with 0 mM (top) and 200 mM NaCl (bottom). The root bending angle is indicated in curved white lines. g, gravity axis.

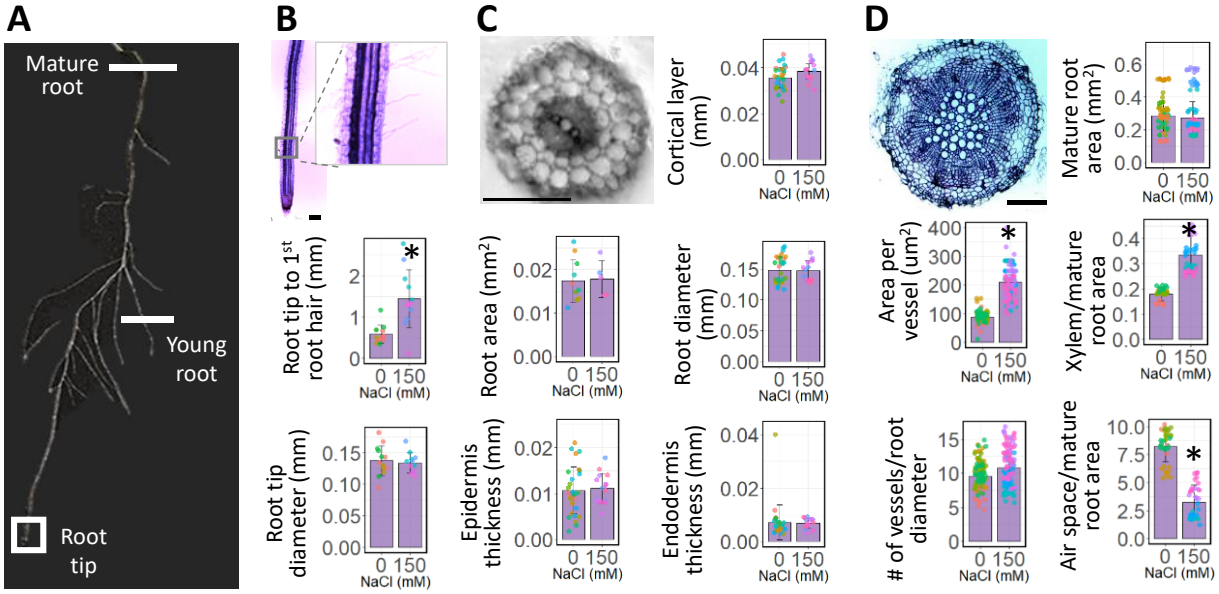

Figure 3. Effects of NaCl stress on *S. parvula* root structures. **[A]** The position of the transverse sections on the *S. parvula* root. Measurements from **[B]** root tip, **[C]** young root, and **[D]** mature root from 12-week-old hydroponically grown *S. parvula* plants. 8-week-old *S. parvula* plants were grown under control or 150 mM NaCl conditions for an additional 4 weeks. A minimum of 20 sections from the mature roots of 4-13 plants were used for mature root quantifications for each condition. 5-10 plants were used for young root quantifications under each condition. The representative cross-sections are from the control plants. Asterisks indicate significant changes ($p \leq 0.05$) between the treated samples and its respective control samples, determined by Student's t-test. Data points represent individual cross-sections and colors represent individual plants. Scale bar represents 100 µm.

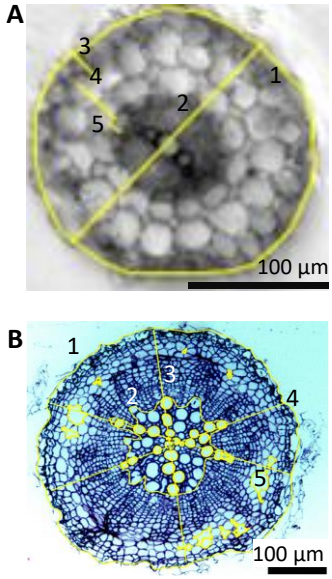

Figure S4. Root structures of *S. parvula*. **[A]** Transverse section of the young root taken at 1-3 cm from the root tip. [1] Young root area; [2] root diameter; [3] epidermis thickness; [4] cortical layer thickness; [5] endodermis thickness. **[B]** Transverse section of the mature root taken between 2-5 cm below the root-shoot junction. [1] Mature root area; [2] xylem/root area; [3] Area per root vessel; [4] # vessel/root diameter; [5] Air space/root area.

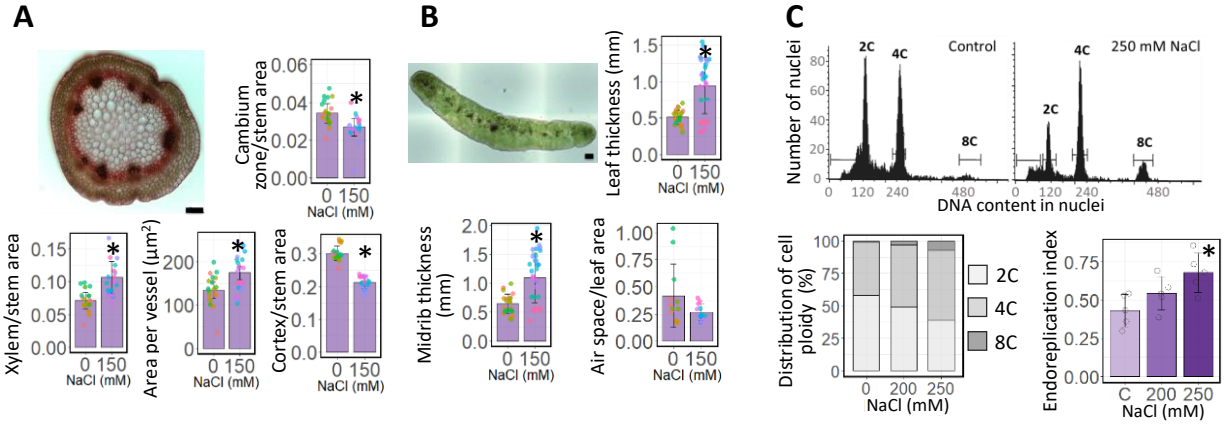

Figure 4. Effects of NaCl stress on *S. parvula* shoot structures. Transverse section of **[A]** stem and **[B]** leaf of 12-week-old hydroponically grown *S. parvula* plants. 8-week-old *S. parvula* plants were grown under control or 150 mM NaCl conditions for an additional 4 weeks. A total of 23 sections from 7 control plants and 32 sections from 9 treated plants were used for leave measurements, a minimum of 20 sections from 5-11 plants were used for stem measurements. Data points represent individual cross-sections and colors represent individual plants. **[C]** Nucleus DNA content, distribution of leaf cell ploidy, and endoreplication index of leaf cells from control and 250 mM NaCl-treated 8-week-old *S. parvula* plants. Data are represented as mean of 4 independent replicates taken from 10th and 11th leaves from the shoot apex. The representative cross-sections are from the control plants. Asterisks indicate significant changes ($p \leq 0.05$) between the treated samples and its respective control samples, determined by Student's t-test. Scale bars represent 100 µm.

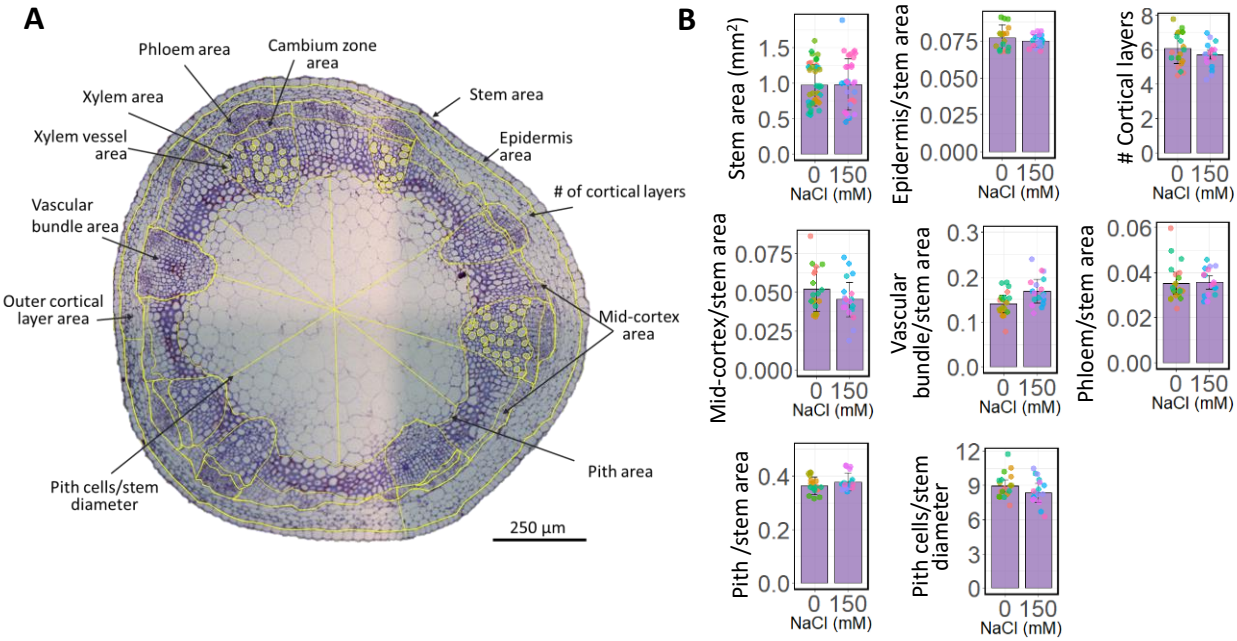

Figure S5. Stem structures of *S. parvula*. **[A]** Transverse section of *S. parvula* stem (between 4th, 5th, and 6th internodes from the shoot meristem) with cell layers marked in yellow lines for trait quantification. **[B]** Measurements for stem anatomical features indicated in A. A minimum of 20 sections from 5-11 plants were used for each measurement. Asterisks indicate significant changes ($p \leq 0.05$) between the treated samples and its respective control samples, determined by Student's t-test. Data points represent individual cross-sections and colors represent individual plants.

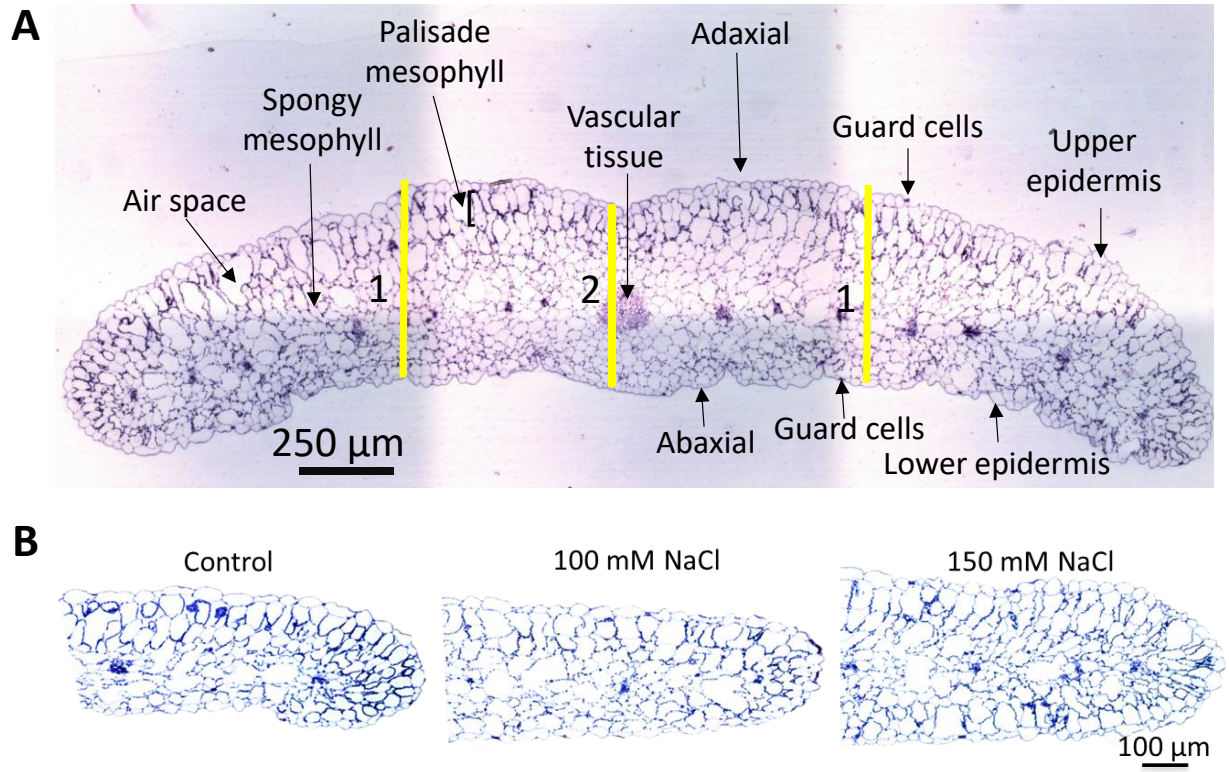

Figure S6. Leaf structures of *S. parvula*. **[A]** Transverse section of *S. parvula* leaves. [1] leaf thickness, [2] midrib thickness. **[B]** Transverse sections of *S. parvula* leaves treated with indicated concentration of salts. All sections come from 5th or 6th leaf from the root-shoot junction in 8-week-old plants that were treated for 4 weeks.

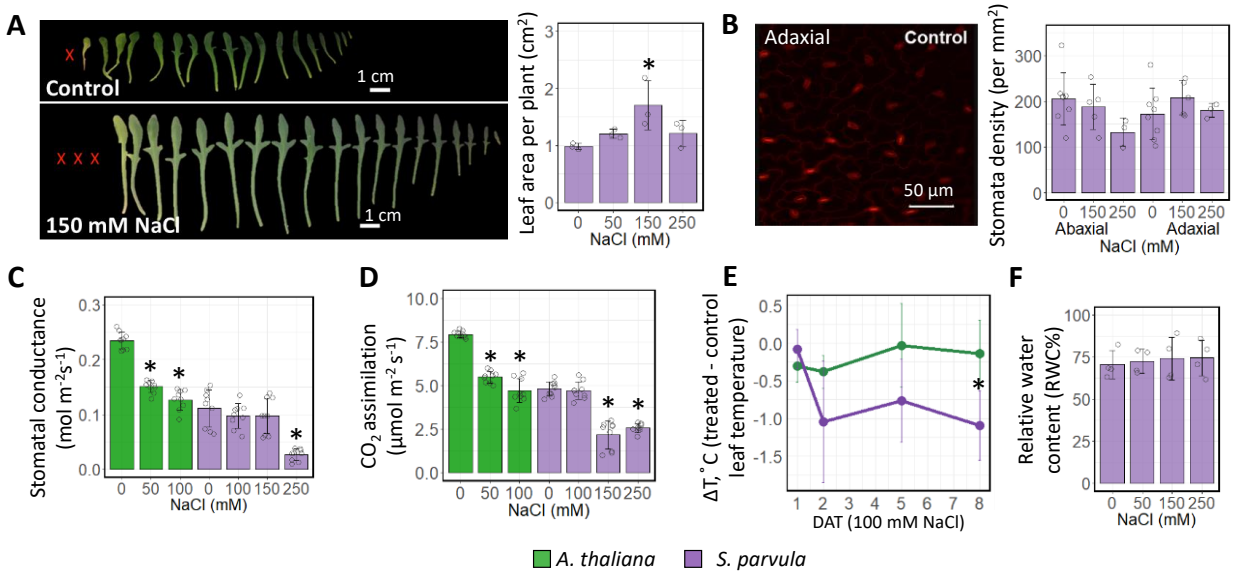

Figure 5. Effects of NaCl stress on *S. parvula* leaves. **[A]** Total photosynthetic leaf area. **[B]** Stomatal density. **[C]** Stomatal conductance. **[D]** Photosynthesis rate. **[E]** Leaf surface temperature. **[F]** Leaf relative water content. All experiments were performed with 4-week-old hydroponically grown plants that were treated for an additional 4 weeks with indicated NaCl concentrations. Asterisks indicate significant changes ($p \leq 0.05$) between the treated samples and its respective control samples, determined by Student's t-test. Data are represented as mean of at least 3 independent replicates ± SD. Open circles indicate number of plants (in B, F, and G) and leaves (in C and D) for each experiment. DAT, days after treatment.

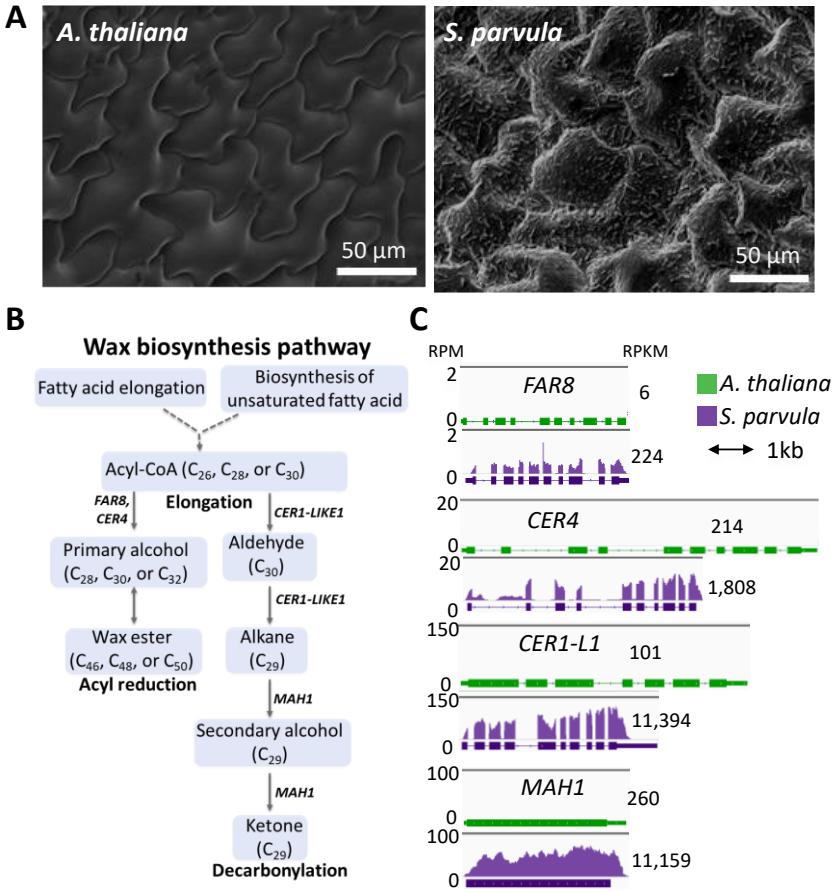

Figure S7. Leaf surface and the basal expression of genes involved in wax biosynthesis in *S. parvula* and *A. thaliana*. **[A]** Scanning electron micrographs contrasting *A. thaliana* and *S. parvula* leaf surfaces. **[B]** Wax biosynthesis pathway and **[C]** wax biosynthesizing gene that were significantly differently expressed between *S. parvula* and *A. thaliana* at basal level (Oh et al., 2014).

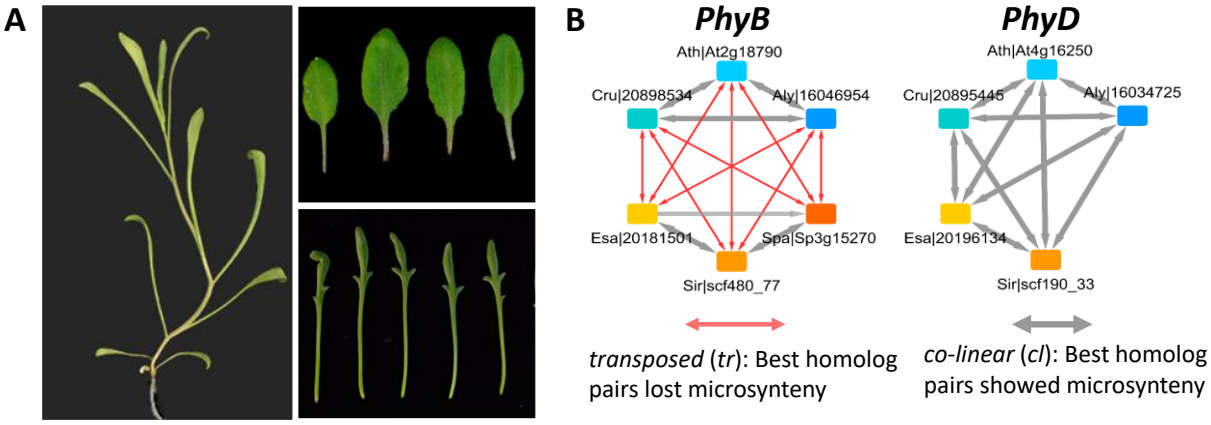

Figure S8. Potential genomic clues for the elongated internode and petiole in *S. parvula*. **[A]** Elongated internode and leaf petiole in *S. parvula* compared to *A. thaliana*. **[B]** *PhyD* is missing in *S. parvula* genome. OrthNet representing evolutionary histories of orthologous gene groups derived from the six Brassicaceae genomes used in Oh and Dassanayake, 2019. Nodes are color-coded according to the species. Edges show properties either co-linear (*cl*) or transposed (*tr*).

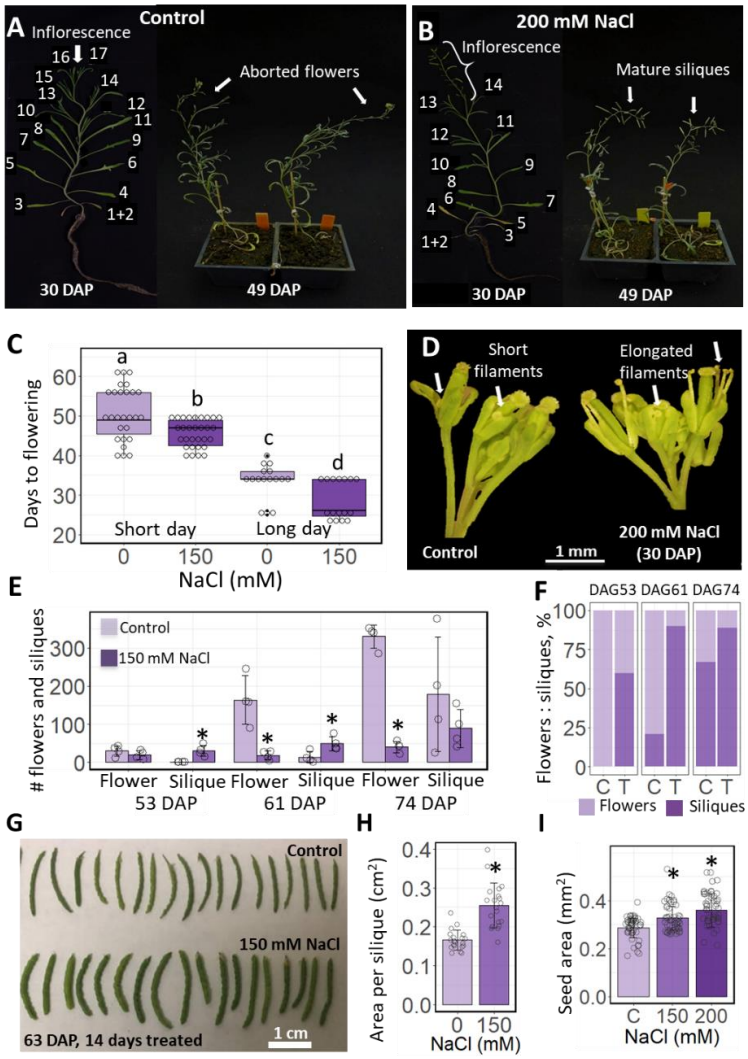

Figure 6. Effects of NaCl stress on fitness of *S. parvula*. **[A]** Plants grown under control conditions generally flower at ~17th leaf stage and the first few flowers are subsequently aborted. **[B]** Salt treated plants flower earlier at ~14th leaf stage and the first flowers develop into mature siliques. **[C]** Days from planting to the first observed flower of plants grown in long day (16 h light/8 h dark) and short day (12 h light/12 h dark). **[D]** Filament length in flowers obtained from control and treated plants. **[E]** Number of flowers and siliques per plant under control and treatment conditions. Open circles represent 4 biological replicates (n=5 plants per replicate). **[F]** Ratio between the number of flowers and siliques observed for control (C) and salt-treated (T) plants used in D. **[G and H]** Comparison of silique size from plants under control and NaCl stress conditions. Open circles represent 20 siliques from 10 plants. **[I]** Comparison of the area of seeds from plants under control and NaCl stress conditions. Open circles represent 50 seeds per treatment from 15-50 plants. For panel [B], the treatment started 21 DAP, initially at 50 mM, included in the water given every other day. The salt concentration increased by 50 mM every four days until reaching 200 mM; for panel [C,E,F], the treatment started on 3-week-old plants until the end of the experiment; for panel [G,H,I], the treatment started on 5-week-old plants, treated for additional 2 weeks. Different letters or asterisks represent significant differences (*, $p < 0.05$) compared to control, determined by either one-way ANOVA followed by either one-way ANOVA followed by Tukey's post-hoc tests [C] or Student's t-test [E, H, I]. DAP, days after planting.

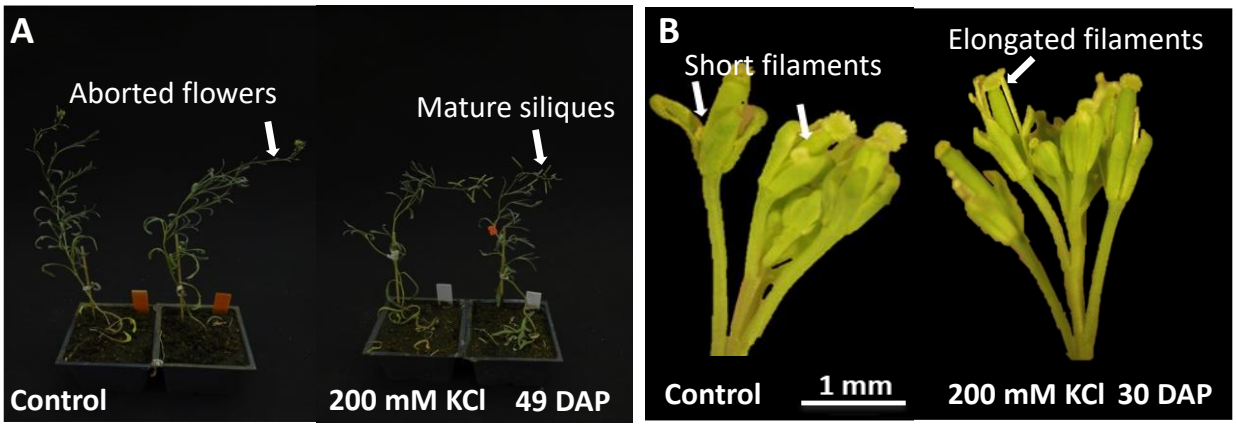

Figure S9. Effects of KCl stress on the fitness of *S. parvula*. **[A]** Plants grown under control conditions generally flower late and the first few flowers are subsequently aborted. KCl treated plants flower earlier and the first flowers develop into mature siliques. **[B]** Early flowers in KCl treated plants develop longer filaments compared to control plants. DAP, days after planting. Note that the control samples shown are the same as Fig 6A.

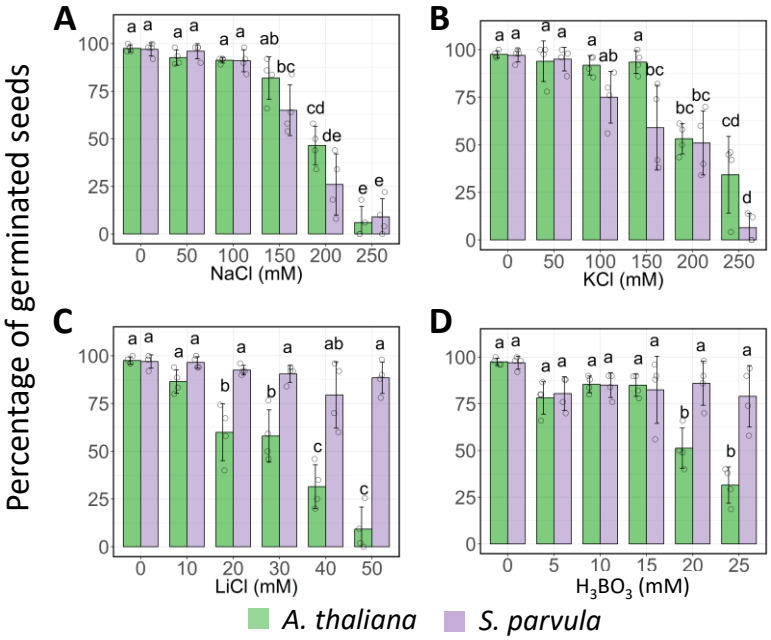

Figure 7. Effects of toxic levels of salts on the germination of *S. parvula* and *A. thaliana* seeds. **[A]** NaCl, **[B]** KCl, **[C]** LiCl, and **[D]** H_3BO_3. The gemination was recorded three days after planting. Different letters indicate significant differences ($p \leq 0.05$) determined by one-way ANOVA with post-hoc Tukey's test. Data are represented as mean of 4 independent replicates ± SD (50 seeds per replicate). Open circles indicate the biological replicates.

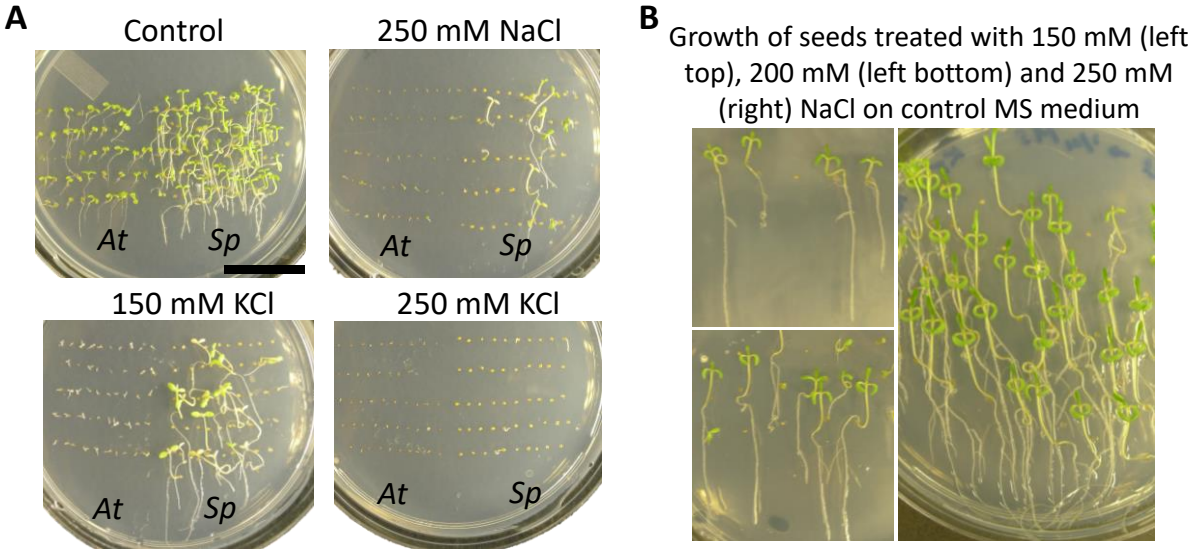

Figure S10. **[A]** *S. parvula* (*Sp*) and *A. thaliana* (*At*) seed germination and growth on NaCl and KCl plates. Scale bars are 2 cm. **[B]** Growth of ungerminated *S. parvula* seeds treated with different concentrations of NaCl (as shown in Figure 7) after transferring to control MS medium.

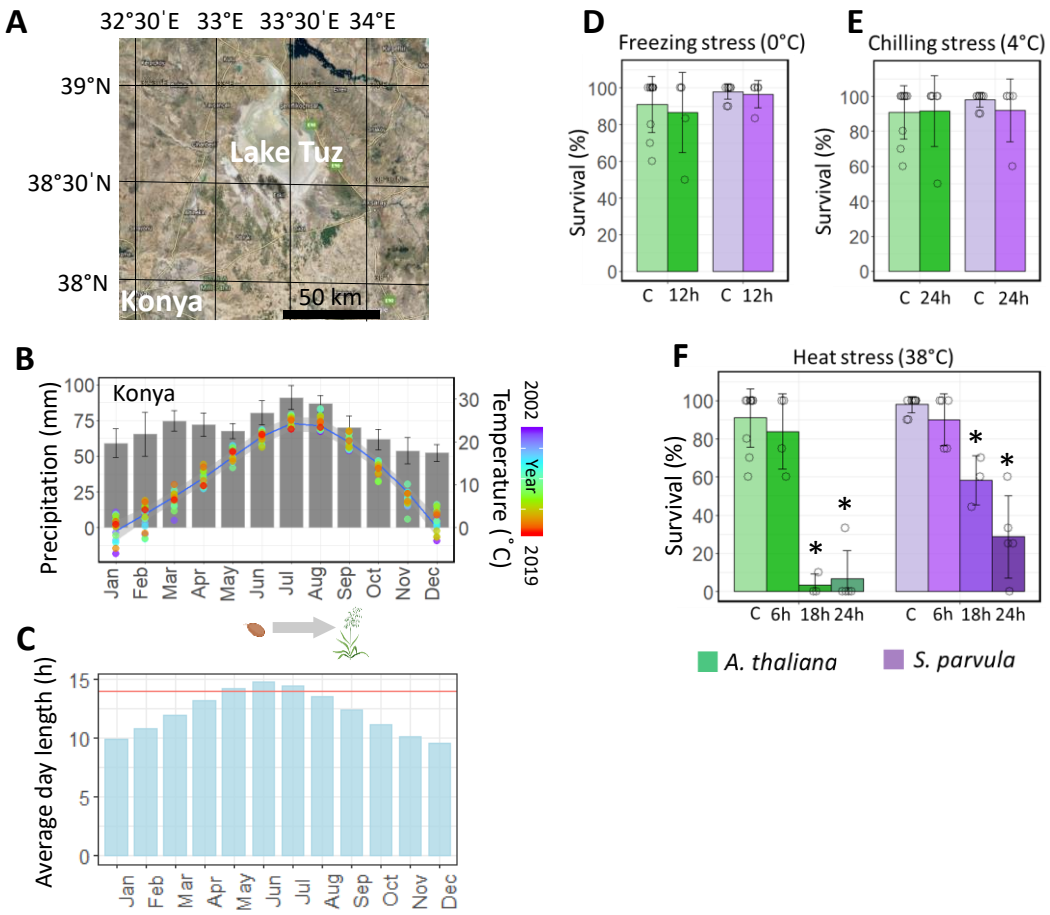

Figure S11. Climate in the Lake Tuz region. **[A]** Lake Tuz location from Google Earth. **[B]** Precipitation and temperature recorded in Konya, Turkey. *S. parvula* life cycle is from April/May to August/September (Tug et al., 2019) (NOAA, 2019). Bars indicate precipitation and lines represent temperature in each plot. **[C]** Average day length recorded in Konya per month. Red line indicated the day length used for plant growth in the lab setting. **[D-F]** Survival rate of *S. parvula* under **[D]** freezing stress, **[E]** chilling stress, and **[F]** heat stress compared to *A. thaliana*. 5-day-old seedlings were subjected to temperature treatments and data were recorded 5 days after recovery. Asterisks indicate significant changes between the treated samples to its respective control samples using t-test with $p \leq 0.05$. Data are represented as mean of 4 independent replicates ± SD (n = 3-6 plants per replicate). Open circles indicate the biological replicates.

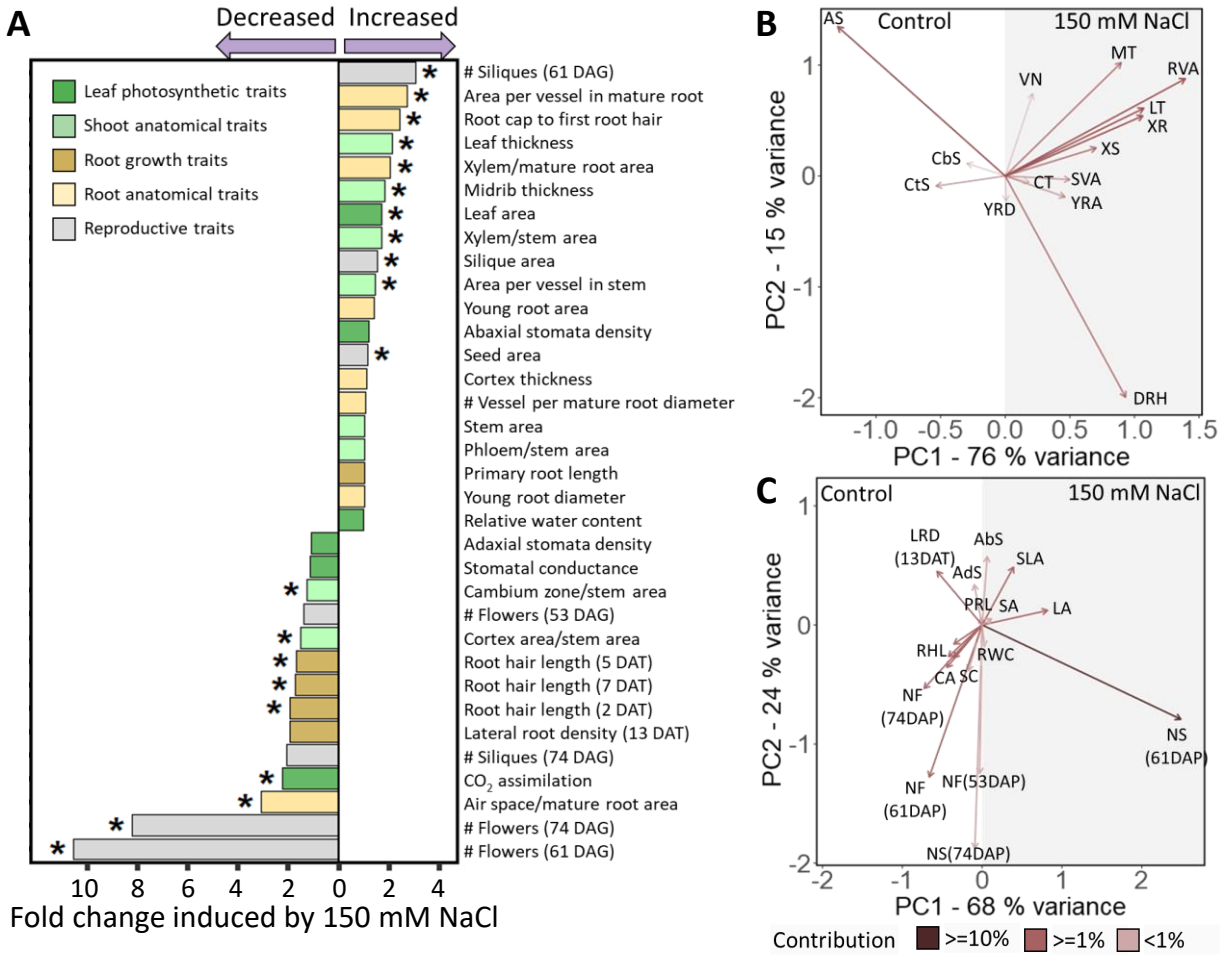

Figure 8. Salt stress induced structural and physiological changes in *S. parvula*. **[A]** Salt stress induced fold changes of traits quantified in the current study. Asterisk represents significant differences (*, $p < 0.05$) compared to control determined by Student's *t*-test. **[B]** and **[C]** PCA biplot of traits quantified for *S. parvula* under control and salt-stressed conditions in current study. [B] Anatomical traits quantified: LT, Leaf thickness; MT, Midrib thickness; XS, Xylem/stem area; SVA, Area per stem vessel; CbS, Cambium zone/stem area; CtS, Cortex/stem area; XR, xylem/root area; RVA, Area per root vessel; VN, # vessel/root diameter; AS, Air space/root area; YRA, Young root area; CT, Cortical thickness; YRD, Young root diameter; DRH, Root tip to 1st root hair, [C] Physiological traits quantified: AbS, Abaxial stomatal density; AdS, Adaxial stomatal density; LA, leaf area; SLA, silique area; SA, seed area; PRL, primary root length; LRD, lateral root density; RWC, relative water content; CA, CO2 assimilation; SC, stomatal conductance; RHL, root hair length; NF, number of flowers; NS, number of siliques. DAT, days after treatment; DAP, days after planting.